Astronomy & Astrophysics manuscript no. Bstars˙orion˙acc
November 2, 2009

The chemical composition of the Orion star forming region

I. Homogeneity of O and Si abundances in B-type stars ⋆

S. Simón-Díaz[1,2]

[1] Instituto de Astrofísica de Canarias, E38200 La Laguna, Tenerife, Spain.
[2] Departamento de Astrofísica, Universidad de La Laguna, E-38205 La Laguna, Tenerife, Spain.

Received; accepted

ABSTRACT

Context. Recent accurate abundance analyses of B-type main sequence stars in the solar vicinity has show that abundances derived from these stellar objects are more homogeneous and metal-rich than previously thought.
Aims. We investigate wether the inhomogeneity of abundances previously found in B-type stars in the Ori OB1 association is real (and hence a signature of enrichment of the newly formed stars in an induced star formation scenario) or a consequence of intrinsic errors induced by the use of photometric indices to establish the stellar parameters prior to the abundance analysis.
Methods. We obtain a new (improved) spectroscopic data-set comprising 13 B-type stars in the various Ori OB1 associations, and perform a detailed self-consistent spectroscopic abundance analysis by means of the modern stellar atmosphere code FASTWIND.
Results. We detect systematic errors in the stellar parameters previously determined which affect the derived abundances. Once these errors are accounted for, we find a high degree of homogeneity of O and Si abundances for stars in the four Ori OB1 subgroups. The derived abundances are in very good agreement with recent determinations in other B-type stars in the solar vicinity. We also compare our results with those obtained for the Sun during the epoch of the "solar crisis", and the Orion nebula.

Key words. stars: early type — stars: atmospheres — stars: fundamental parameters — stars: abundances

1. Introduction

1.1. Abundances of B-type stars in the solar vicinity

For many years, our knowledge about the chemical composition of early-B main sequence stars in the solar vicinity was characterized by two main results: the derived abundances seemed to be highly inhomogeneous (with a dispersion of up to 0.5 dex), and the mean values indicated lower abundances than the standard (Grevesse & Sauval, 1998) set of solar abundances (see reviews by Herrero & Lennon, 2004; Morel, 2009). These results were not very encouraging; the inhomogeneity of stellar abundances was in contradiction with the homogeneity in oxygen abundance found from the study of the local diffuse interstellar medium (e.g. Meyer, Jura, & Cardelli, 1998; Cartledge et al., 2006). On the other hand, chemical evolution models of the Galaxy (e.g. Chiappini, Romano, & Matteucci, 2003; Carigi et al., 2005) predict a small enrichment of the ISM in metals during the lifetime of the Sun (i.e. nearby OB-type stars, being younger than the Sun, are expected to be slightly metal-rich).

Some recent results have began to change this situation. The solar oxygen abundance traditionally considered as a cosmic abundance reference (Grevesse & Sauval, 1998) was reviewed by Asplund et al. (2004), who obtained log (O/H)=8.66 dex, 0.17 dex lower than the standard value. This was the beginning of what has been called the epoch of the "solar crisis": between 2004 and 2008, several studies by different authors (Ayres et al., 2006; Socas-Navarro & Norton, 2007; Allende Prieto, 2008; Caffau et al., 2008; Ayres, 2008; Meléndez & Asplund, 2008; Centeno & Socas-Navarro, 2008) presented solar oxygen abundances derived by means of different approaches; the calculated values range from 8.63 dex (Socas-Navarro & Norton, 2007) to 8.86 dex (Centeno & Socas-Navarro, 2008). The debate about its actual value is still open.

Przybilla, Nieva, & Butler (2008) recently analyzed a representative sample of six unevolved early B-type stars in nearby OB associations and the field, and found a very narrow distribution of abundances, with mean values more metal-rich compared to previous works (e.g. log (O/H)=8.76 dex, a value that is within the range of solar abundances calculated during

Send offprint requests to: S. Simón-Díaz, e-mail: ssimon@iac.es

⋆ Based on observations made with the Nordic Optical Telescope, operated on the island of La Palma jointly by Denmark, Finland, Iceland, Norway, and Sweden, in the Spanish Observatorio del Roque de los Muchachos of the Instituto de Astrofisica de Canarias.

the "solar crisis"). These authors indicate the importance of a proper determination of the atmospheric parameters and the use of robust model atoms to avoid systematic errors in the abundance determination (see also Nieva & Przybilla, 2009, for a summary of the main sources of systematic errors affecting the abundance analyses of B-type stars). The study by Przybilla, Nieva, & Butler show that the chemical inhomogeneity previously found for B-type stars in the solar vicinity may be spurious, and a artificial effect of those systematic errors. It also reinforces the importance of self-consistent spectroscopic abundance analyses (i.e. the stellar parameters and the metal abundances are determined exclusively from spectroscopic diagnostics by using the same set of stellar atmosphere models); less accurate photometric $T_{\rm eff}$ estimates must be handle with care (or better avoided whenever possible!) in the abundance analysis of B-type stars (see also Nieva & Przybilla, 2008).

1.2. The Orion star forming region (Ori OB1)

The Orion complex, containing the Orion Molecular Cloud and the Orion OB1 (Ori OB1) association, is one of the most massive active star forming regions in the 1 kpc centered on the Sun. Blaauw (1964) divided Ori OB1 into four subgroups of stars — namely Ia, Ib, Ic, and Id — having different locations in the sky and ages. Brown et al. (1994) derived mean ages of 11.4±1.9, 1.7±1.1[1], 4.6±2, and <1 Myr for subgroups Ia to Id, respectively. The youngest subgroup Ori OB1 Id is associated with the Orion nebula (M 42), the most studied H II region and the closest ionized nebula to the Sun in which a high accuracy abundance analysis can be performed.

The correlation between the ages of the stellar subgroups, their location, and the presence of large scale structures of the interstellar medium around Orion OB1 have been interpreted as features of sequential star formation and Type-II supernovae (Reynolds & Ogden, 1979; Cowie et al., 1979; Brown et al., 1994). Cunha & Lambert (1992, 1994) obtained C, N, O, Si, and Fe abundances of 18 B-type main sequence stars from the four subgroups comprising the Ori OB1 association. They found a range in oxygen abundances[2] of ∼0.4 dex, with the highest values corresponding to the stars in the youngest (Id and some Ic) subgroups. In this case, the inhomogeneity in stellar abundances (mainly oxygen and silicon) seemed to be real and coherent with a scenario of induced star formation in which the new generation of stars are formed from interstellar material contaminated by Type-II supernovae ejecta.

The study by Cunha & Lambert was based on a photometric estimation of $T_{\rm eff}$ and the fitting of the Hγ line computed from Kurucz (1979) LTE model atmospheres to the observed one to derive $\log g$. In a more recent work, Simón-Díaz et al. (2006) used one of the new generation of NLTE, line blanketed, model atmosphere codes (FASTWIND, Santolaya-Rey et al., 1997; Puls et al., 2005) and a self-consistent spectroscopic approach to derive the stellar parameters and oxygen abundances for the three B0.5 V stars in Ori OB1d (the youngest and, supposedly, more metal rich subgroup). The resulting stellar parameters were somewhat different and, more importantly, the derived abundances were systematically lower than the previous values by Cunha & Lambert (1994) by ∼ 0.2–0.3 dex.

This result motivated us to review the chemical composition of the other B-type stars in Ori OB1 to investigate whether the inhomogeneity of abundances previously found is real or a consequence of intrinsic errors induced by the use of photometric indices to establish the stellar parameters prior to the abundance analysis. To this aim, we obtained a totally new (improved) observational data-set, and performed a self-consistent abundance analysis of 13 of the stars considered by Cunha & Lambert (1992, 1994).

In this paper we use FASTWINDto derive the stellar parameters, oxygen and silicon abundances. The observational data-set is described in Sect. 2. The whole spectroscopic analysis is presented in Sect. 3. Then, we compare our stellar parameters and abundance with results from previous works (Sect. 4). The homogeneity of stellar abundances in Ori OB1 and its comparison with other B-type stars in the solar vicinity determinations, the Sun, and the Orion nebula is discussed in Sect. 5. The main conclusions of this work are summarized in Sect. 6.

2. Observational data-set

The observations used here were carried out with the FIES cross dispersed high resolution echelle spectrograph attached to the NOT2.5m telescope at El Roque de los Muchachos observatory on La Palma (Islas Canarias, Spain) on 5-8 November 2008. The medium resolution mode (R=46000, $\delta\lambda$=0.03 Å/pix) was selected and the entire spectral range 3700-7300 Å was covered without gaps in a single fixed setting. A sample of 14 stellar candidates, selected from the list of stars in the Ori OB1 association analyzed by Cunha & Lambert (1992, 1994), was observed. These are early-B type, non evolved, stellar objects (B0 V-B2 V) with low projected rotational velocities ($v \sin i \leq 60$ km s^{-1}). The signal-to-noise ratio achieved for all the spectra was always above 250. The list of observed stars is presented in Table 1. Note that, apart from the new set of stars, we re-observed HD 37020 and HD 37042, two of the three B-type stars[3] analyzed in Simón-Díaz et al. (2006).

The spectra were reduced with the FIEStool[4] software in advanced mode. The FIEStool pipeline provided wavelength calibrated, blaze corrected, order merged spectra of high quality. These spectra were then normalized using own developed IDL programs. An example of the FIES@NOTspectra for three of the observed stars is presented in Fig 1, where the Si II-IV and O II lines used for the abundance analysis are also indicated.

[1] Briceño et al. (2005) determined an age for Ori OB1b ∼4 – 6 Myr by studying its low mass, young stellar population; this value is more consistent with what would be expected from the presence the evolved blue supergiant ϵ Ori in this subgroup.

[2] Other authors (Gies & Lambert, 1992; Kilian, 1992; Gummersbach et al., 1998) obtained a similar range in oxygen abundances from the analysis of smaller samples of B-type stars in Orion OB1.

[3] HD 37023 was also re-observed, but it was not included in the analysis because we found in the new spectrum that the star is is actually a binary system (SB2), and hence not optimal for an abundance analysis.

[4] http://www.not.iac.es/instruments/fies/fiestool/FIEStool.html

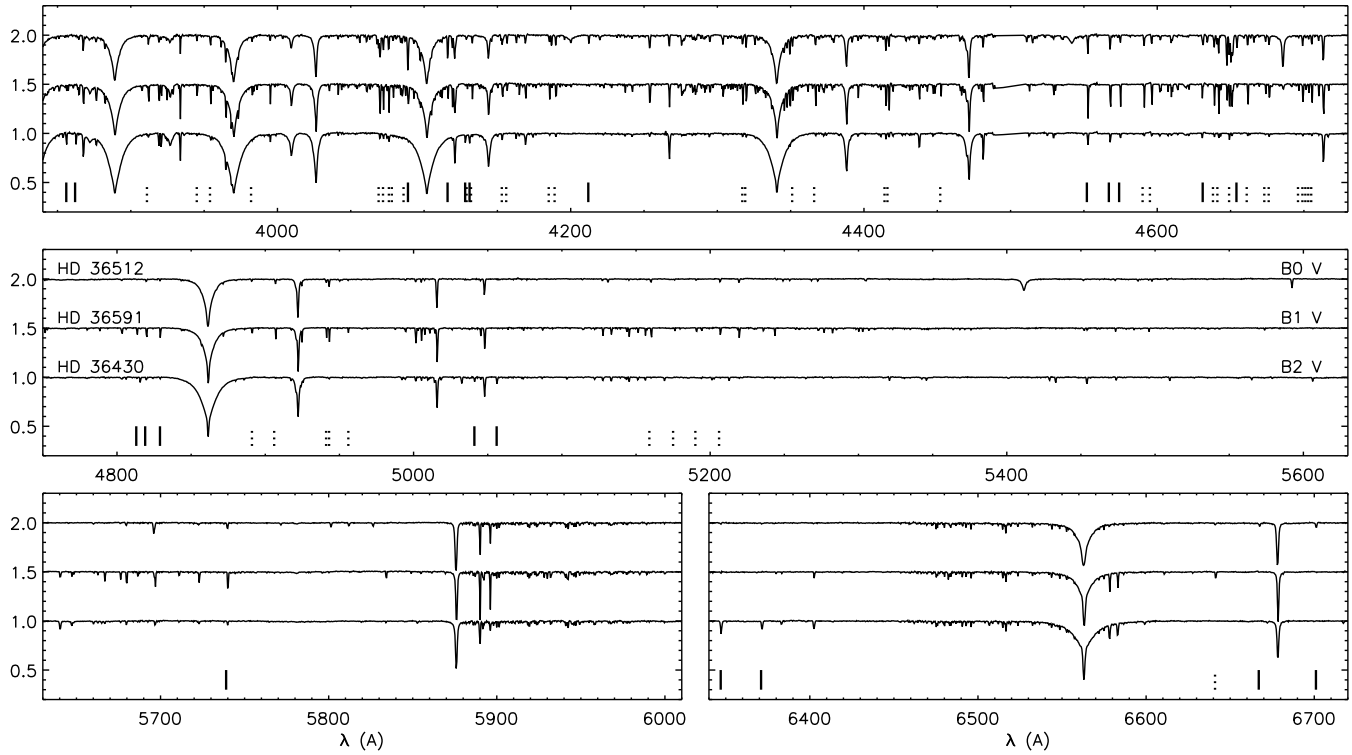

Fig. 1 Example of FIES@NOTspectra for three of the observed stars. The complete atlas is available in the electronic version of the paper (Fig. 10). The Si II-IV and O II lines used for the abundance analysis are indicated as solid and dashed vertical lines, respectively.

3. Spectroscopic analysis

The analyses were performed following a self-consistent spectroscopic approach with the spherically extended, NLTE, line-blanketed stellar atmosphere code FASTWIND (Santolaya-Rey et al., 1997; Puls et al., 2005). Basically, the stellar parameters were derived by comparing the observed H Balmer line profiles and the ratio of Si III-IV and/or Si II-III line equivalent widths with the output from a grid of FASTWIND models. Whenever possible, the He I-II ionizing equilibrium was also considered. Then, the same grid of models was used to derive the stellar abundances by means of the curve of growth method.

3.1. Projected rotational velocities

The projected rotational velocities ($v \sin i$) were obtained by applying the Fourier method (Gray, 1976; see also Simón-Díaz & Herrero, 2007, for its application to OB-type stars) to the Si III λ4552 line. The 0.03 Å/pix resolution of the FIES spectra implies that the lowest $v \sin i$ could be detected is 2-3 km s^{-1}; however, for those cases with $v \sin i <$ 10-15 km s^{-1}, the identification of the first zero of the Fourier transform was difficult due to the effect of the noise (an maybe the microturbulence).

In many cases, an additional extra Gaussian-type broadening (Θ_g) was needed to properly fit the line profile for the derived value of $v \sin i$. This extra-broadening account for the microturbulence (and maybe the macroturbulence), also affecting the shape of the line. The corresponding derived values are summarized in Table 2.

Table 1 List of B-type stars from Ori OB1 considered in this study, ordered by spectral type.

HD	HR	Name	SpT	V	Subgroup
HD 36512	HR 1855	ν Ori	B0 V	4.62	Ic
HD 37020	HR 1893	θ^1 Ori A	B0.5 V	6.71	Id
HD 36960	HR 1887		B0.5 V	4.78	Ic
HD 37042		θ^2 Ori B	B0.7 V	6.02	Id
HD 36591	HR 1861		B1 V	5.34	Ib
HD 36959	HR 1886		B1 V	5.67	Ic
HD 35299	HR 1781		B1.5 V	5.69	Ia
HD 37744	HR 1950		B1.5 V	6.22	Ib
HD 36285	HR 1840		B2 V	6.33	Ic
HD 36629			B2 V	7.65	Ic
HD 35039	HR 1765		B2 V	4.72	Ia
HD 36430	HR 1848		B2 V	6.23	Ic
HD 35912	HR 1820		B2 V	6.41	Ia

3.2. Measurement of equivalent widths and identification of problematic lines

The strategy we followed in our analyses is based in the equivalent widths (EW) of metal lines. Therefore, a proper identification of the lines of interest, along with an accurate measurement of their EWs (also including the associated uncertainties) is a very important step. We have developed IDL rutines to automatically identify metal lines in the spectra, measure the EWs and their uncertainties, and detect the possible presence of other lines affecting these measurements. To this aim we compiled a list of C, N, O, Si, Mg, S, Ne, and Ar lines,

Table 2 Projected rotational velocities derived for the studied stars. In some cases, an extra Gaussian-type broadening Θ_g was needed to reproduce the shape of the line profile. Both quantities in km s^{-1}.

HD	$v \sin i$	Θ_g	HD	$v \sin i$	Θ_g
HD 36512	15	30	HD 37744	37	00
HD 37020	55	00	HD 36285	<10	20
HD 36960	23	40	HD 36629	<10	15
HD 37042	31	00	HD 35039	<12	15
HD 36591	08	19	HD 36430	<15	25
HD 36959	12	12	HD 35912	<12	20
HD 35299	<08	12			

extracted from the atomic[5] line list v2.05. For a given line, the program performs a multi-Gaussian fit of the observed line profile accounting for all the lines expected to be present in a certain spectral range ($\lambda_0 \pm 2 \max[v \sin i \lambda_0/c, 0.5\lambda_0/R]$) around the wavelength indicated in the line list. The uncertainty in the EW measurement is obtained assuming the location of the local continuum at $\pm 1/SNR$ and, in those cases in which the line is isolated, comparing the value obtained by means of the Gaussian fitting with the value derived by integrating the line.

The high quality of our spectra allowed us to identify and measure the EWs of up to 27 Si II-IV lines and 47 O II lines. Some of the lines were labeled as problematic due to the presence of one or more lines from other elements (e.g. the O II λ4673.73 line may be affected by the C III λ4673.95 in same cases; similarly occurs for the O II λ4641.81 line, coincident with the N III λ4641.85 line). These lines were treated with special care in the abundance analysis, as they may be giving wrong values for the abundance.

Generally, the Gaussian fit provide reliable results for the equivalent widths; however, in those cases in which the $v \sin i$ of the star is above 30-35 km s^{-1} the use of a Gaussian to fit the profile may result in an under or overestimation of the EW (in a few percent), depending on the line strength. For those cases the EW resulting from the integration of the observed line profile was preferred.

3.3. A grid of HHeOSi FASTWIND models

For this study, we constructed a grid of FASTWIND models with T_{eff} and $\log g$ ranging from 17 to 36 kK (1 kK steps) and 3.7 to 4.3 dex (0.1 dex steps). As the studied stars are not expected to be evolved, the He abundance was fixed to 0.09 dex. In addition, since FASTWIND is a spherically extended code, the radius and other wind parameters need to be indicated; these are grouped in the Q-parameter. We fixed this parameter to $\log Q = -15$ as a representative value for which the wind effect over the optical spectrum is practically negligible (Hα and He IIλ4686 show no sign of wind contamination). The metallicity was assumed to be solar (following the set of abundances by Grevesse & Sauval, 1998), and a microturbulence of 15 km s^{-1} was considered in the stellar atmosphere structure calculation.

[5] http://www.pa.uky.edu/~peter/newpage/

For each pair of stellar parameters, a sub-grid of models varying the microturbulence (ξ_t = 1, 3, 5, 7, 9 km s^{-1}), the Si abundance (ϵ_{Si} = –5.10, –4.80, –4.50, –4.20 dex), and the O abundance (ϵ_O = –4.00, –3.65, –3.30, –2.95 dex) was calculated. The O and Si atomic models used for the grid came mainly from Becker & Butler (1988, 1990). However, two updates were considered: (a) a extended Si II model atom (see Trundle et al., 2004), and (b) we used the most recent log gf values indicated in the atomic line list v2.05 for the formal solution calculations.

The final grid consists of 20x7x4 (=560) models and a total of 2800 formal solutions (5 microturbulence values per model). It includes line profiles and equivalent widths for H, He I-II, Si II-IV and O II lines, along with the spectral energy distribution (SED) for each set of stellar parameters.

3.4. Stellar parameter determination

The use of the Si III-IV and/or Si II-III ionization equilibrium, along with the H Balmer lines, for the determination of the stellar parameters of early B-type stars is a longstanding method described elsewhere (see e.g. Kilian et al., 1991; Urbaneja et al., 2005; Crowther et al., 2006; Markova & Puls, 2008). The ratios EW(Si IV λ4116)/EW(Si III λ4552) and/or EW(Si II λ4128)/EW(Si III λ4552), depending on the temperature of the star have been traditionally used as T_{eff} indicators. This decision has been probably motivated by the fact that these are the strongest, not blended lines in the spectral range commonly observed for the stellar abundance analysis (i.e. ~ 4000 – 5000 Å).

We derived the stellar parameters, along with the Si abundance, for all stars in our sample using this methodology. We initially considered the abovementioned Si line ratios to determine the effective temperatures (columns 3 and 4 in Table 3). However, motivated by a couple of problems we found when deriving the stellar parameters in the cooler objects (see discussion below), we decide to also include as a temperature indicator the EW(Si II λ6347)/EW(Si III λ4552) ratio (column 5). The measured values are indicated in brackets in the corresponding columns. As expected, the Si IV/Si III ratio decreases when we move to latter spectral types and the Si II/Si III behaves in a opposite way. For three of the stars (HD 36959, HD 35299, and HD 37744), lines from the three ions are simultaneously clearly present in the spectra.

Four parameters need to be determined at the same time in an iterative way: T_{eff}, $\log g$, ξ_t(Si), and ϵ_{Si}. Firstly, we use the Si line ratios indicated above and the wings of the H Balmer lines (fixing ξ_t(Si), and ϵ_{Si}) to obtain a initial guess for T_{eff} and $\log g$. Then we apply the curve of growth method to a proper set of Si II-IV lines to iteratively obtain final values for the four parameters (a detailed description of the used lines and the results of the Si abundance analysis is presented in sections below). Normally, the final values of T_{eff} and $\log g$ are quite close to the initial values, since the mentioned line ratios are only slightly dependent on ϵ_{Si} and ξ_t.

Table 3 Final results of the HSi analysis: stellar parameters and Si abundances. Detailed results (line-by-line) of the Si abundance analysis are presented in Tables 6 to 18 in the electronic version of the paper. Four different T_{eff} indicators were used whenever possible; one of them refers to He I-II lines and the other three to Si II-IV lines. For the Si cases, the ratios of equivalent width are indicated in brackets above the derived T_{eff} (EW_4: Si IV 4116; EW_3: Si III 4552; EW_{2A}: Si II 4130; EW_{2B}: Si II 6371). All T_{eff} values correspond to the $\log g$ indicated in the 8th column. Errors associated with the adopted T_{eff} and $\log g$ (columns 7 and 8) are 500 K and 0.1 dex, respectively (see text). Last column illustrates the effect of a change of ±500 K on the derived Si abundance when only Si III are used.

		(EW_4/EW_3)	(EW_{2A}/EW_3)	(EW_{2B}/EW_3)		Adopted				T_{eff}±500 K
Target	SpT	T_{eff} – Si IV-III	T_{eff} – Si II-III	T_{eff} – Si II-III	T_{eff} – He I-II	T_{eff}	$\log g$	ξ_t(Si)	$\epsilon_{Si}\pm\Delta\epsilon_{Si}[\sigma, \xi_t]$	$\Delta\epsilon_{Si}$ (Si III)
		(1.42±0.06)								
HD 36512	B0 V	33700±200	...	...	34000±500	**33700**	**4.2**	4.3±0.7	**7.49**± [0.07, 0.05]	±0.12
		(0.69±0.09)								
HD 37020	B0.5 V	30500±600	...	...	30000±500	**30500**	**4.2**	0.5±0.5	**7.47**± [0.10, 0.04]	±0.06
		(0.60±0.04)								
HD 36960	B0.5 V	28900±300	...	...	29000±500	**28900**	**3.9**	5.4±0.6	**7.53**± [0.02, 0.06]	±0.06
		(0.64±0.07)								
HD 37042	B0.7 V	29700±400	...	...	29500±500	**29700**	**4.2**	1.4±0.3	**7.55**± [0.03, 0.04]	±0.05
		(0.39±0.01)								
HD 36591	B1 V	27200±100	...	...	...	**27200**	**4.1**	1.3±0.3	**7.53**± [0.06, 0.03]	±0.01
		(0.25±0.02)	(0.12±0.02)							
HD 36959	B1 V	25900±300	25900±100	...	...	**25900**	**4.2**	0.0±1.0	**7.50**± [0.05, 0.07]	∓0.02
		(0.16±0.03)	(0.12±0.01)	(0.12±0.04)						
HD 37744	B1.5 V	23900±600	25700±100	23600±600	...	**23800**	**4.1**	0.5±0.5	**7.54**± [0.06, 0.04]	∓0.05
		(0.14±0.02)	(0.20±0.01)	(0.17±0.03)						
HD 35299	B1.5 V	23900±300	24900±300	23700±300	...	**23700**	**4.2**	0.5±0.5	**7.50**± [0.08, 0.02]	∓0.06
			(0.26±0.01)	(0.41±0.03)						
HD 36285	B2 V	...	23900±200	20600±200	...	**20600**	**4.0**	1.7±0.5	**7.49**± [0.06, 0.05]	∓0.11
			(0.36±0.02)	(0.44±0.04)						
HD 35039	B2 V	...	22200±200	19900±200	...	**19800**	**3.7**	3.3±1.0	**7.52**± [0.06, 0.08]	∓0.14
			(0.39±0.02)	(0.53±0.02)						
HD 36629	B2 V	...	22800±300	20000±100	...	**20000**	**4.1**	1.0±0.5	**7.54**± [0.04, 0.05]	∓0.13
			(0.65±0.06)	(0.96±0.09)						
HD 36430	B2 V	...	21000±300	18600±200	...	**18600**	**4.1**	3.5±1.0	**7.47**± [0.08, 0.07]	∓0.13
			(0.73±0.05)	(0.92±0.05)						
HD 35912	B2 V	...	20400±300	18500±150	...	**18500**	**4.0**	3.2±0.5	**7.48**± [0.07, 0.04]	∓0.13

3.4.1. Hotter objects ($T_{eff}\geq$ 27000 K)

In the hotter objects Si II lines are not present in the spectra. The EW(Si IV λ4116)/EW(Si III λ4552) ratio is hence used to obtain the initial guess values of T_{eff} for each of the $\log g$ values considered in the grid. Then, the full set of reliable Si III-IV lines, along with the H Balmer line profiles is used for the fine determination of the four parameters indicated above (see an example in the upper panel of Fig. 2, and in Fig. 3). Note that the uncertainties in the EW measurements of the Si lines have been taken into account to establish the uncertainties associated with the derived stellar parameters. Generally, the T_{eff} and $\log g$ can be determined with an accuracy better than 500–600 K and 0.1 dex, respectively. The final results of the analysis are presented in Table 3.

For main sequence stars with $T_{eff} \gtrsim 28000$ K the He I-II ionization equilibrium can be also used (see e.g. Herrero et al., 1992; Simón-Díaz et al., 2006). (Below this temperature, He II lines are too faint or not present in the spectrum.) We could determine the stellar parameters in this way for four of the stars in our sample. An example of this type of analysis was already presented in Simón-Díaz et al. (2006), and hence we only present here the corresponding results (see column 6 in Table 3). In general, there is a good agreement between the T_{eff} determined through the Si III-IV and the He I-II ionization balance (with differences in T_{eff} not larger than ∼500 K.

3.4.2. Cooler objects

For the cooler objects, the Si II/Si III must be used. We initially considered the EW(Si II λ4130)/EW(Si III λ4552) ratio to obtain a first estimation of the stellar parameters; however, we found two facts that warned us about a possible problem with the Si II λ4130 (or the Si II λ4128) line. Firstly, it was not possible to properly fit the H Balmer lines for any of the (T_{eff}, $\log g$)-pairs indicated by the Si II λ4130/Si III λ4552 line ratio; the core of the H synthetic lines resulted somewhat narrower than the observed ones (even if large values of $\log g$ are considered). Note that for these temperatures the cores of the H Balmer lines begin to be sensitive to changes in T_{eff}. For all the studied cases, these lines require somewhat lower effective temperatures to properly fit their cores. Secondly, the ϵ_{Si}-EW diagnostic diagrams showed two sets of Si II lines giving different abundances by ∼0.2 dex (see lower pannel in Figure 2). Curiously, each subset of lines corresponds to transitions with very different en-

ergy levels (Si II $\lambda\lambda$4128, 4130, 5041, 5056 in one hand, coming from higher energy levels; Si II $\lambda\lambda$6347, 6371, 3856, 3862 on the other hand, resulting from lower energy levels; we suggest the reader to have in hand a Grotrian diagram). This different behavior of the various lines warned us about possible problems with the Si II atomic model and the use of Si II λ4128 line alone to establish the stellar temperature.

Columns 4 and 5 in Table 3 show the different effective temperatures obtained depending of the Si II line which is used (Si II λ4128, Si II λ6371. Temperatures given by the EW(Si II λ6371)/EW(Si III λ4552) ratio are systematically lower by up to ~2000 – 3000 K. In addition, with these new values of the temperature, a proper fit of the cores of the H Balmer lines can be achieved.

3.4.3. HD 36595, HD 37744, and HD 35299

These three stars show Si II-III-IV lines in their spectra, and hence can contribute with new decisive clues for the problem mentioned above. In this case we count with three $T_{\rm eff}$ indicators. As can be noticed from inspection of Table 3, the $T_{\rm eff}$ indicated by the EW(Si II λ6371)/EW(Si III λ4552) ratio results in a better agreement than the other Si II/Si III ratio for two of the three cases. For the hotter object (HD 36959) the Si II λ6371) is too faint to be measured; although the $T_{\rm eff}$ indicated by the EW(Si II λ4130)/EW(Si III λ4552) ratio agrees with the Si IV/Si III diagnostic in this object, this is not the case for the other objects.

In Fig. 2 (middle pannel) we show the $\epsilon_{\rm Si}$-EW diagnostic diagram for the case of HD 37744. The stellar parameters considered in this plot are those indicated by the Si IV/Si III ratio. The Si II $\lambda\lambda$6371, 3856 lines perfectly fit with the other Si III-IV lines, but not the Si II $\lambda\lambda$4128, 4130 lines.

3.4.4. Concluding

We found some indications pointing towards a problem in the Si II model atom which result in a bad modeling of the Si II $\lambda\lambda$4128, 4130, 5041, 5056 lines. Fortunately, our observations also include other Si II lines which seems to behave in a proper way. A review of the Si II model atom is needed (which could be tested with the type of detailed analysis presented here), but in the meantime, several arguments allow us to trust[6] in the Si II $\lambda\lambda$6347, 6371, 3856, 3862 set of lines for the stellar parameters determination and abundance analysis of the cooler objects in our sample: (a) the coherence of results between Si IV-III and Si III-II in terms of $T_{\rm eff}$; (b) the good fit of the H Balmer lines for the cooler stars when the lower $T_{\rm eff}$ is considered; (c) as we will show in the next section, when this solution is adopted a coherence of results in Si and O abundances is found for all the stars in our sample.

[6] This hypothesis is also supported by a comparison of $T_{\rm eff}$ obtained for the cooler objects in our sample from other spectroscopic diagnostic based in O II/I and C III/II ratios of lines (F. Nieva, private communication).

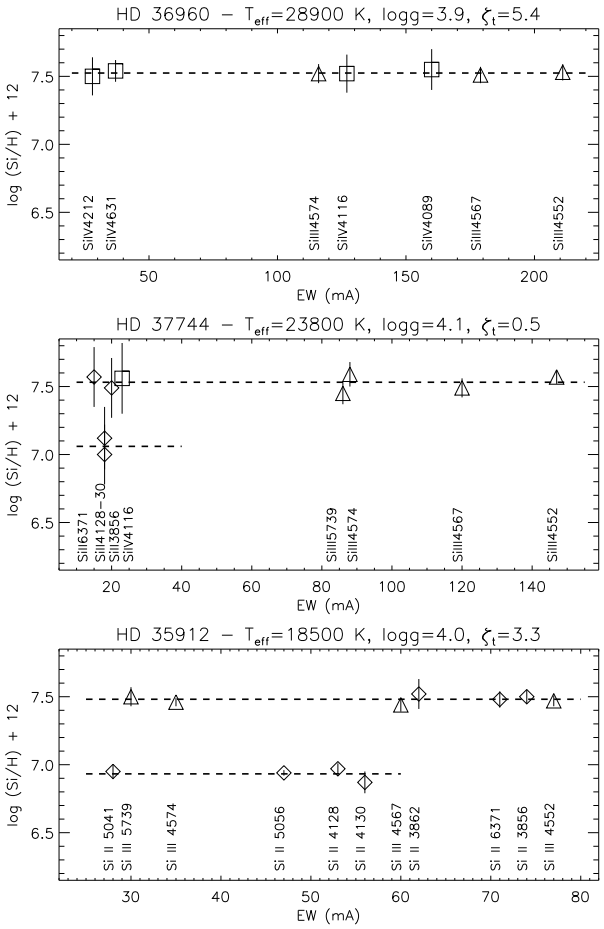

Fig. 2 Silicon abundance vs. equivalent width diagnostic diagrams for three of the analyzed stars (with representative effective temperatures).

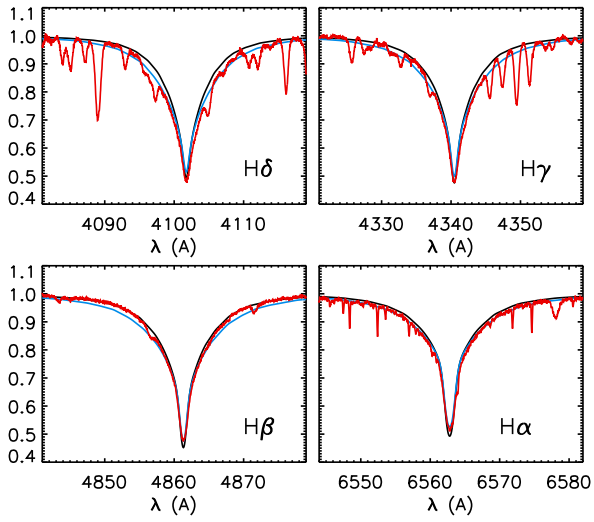

Fig. 3 Example of fitting of the H Balmer lines to determine $\log g$. Two FASTWIND models are compared with the observed spectrum (red line) of HD 36960: in black, model with the stellar parameters resulting from the FASTWIND HSi analysis (28900, 3.9); in blue, model with the stellar parameters derived by Cunha & Lambert (1992), for comparison (28900, 4.3).

3.4.5. Uncertainties

Columns 3 and 5 indicate the uncertainties in T_{eff} obtained from the consideration of errors in the equivalent widths measurement of Si II-IV lines. These uncertainties, obtained by assuming a fixed gravity are ∼100-600 K. Gravity can be normally established with an accuracy better 0.1 dex. Uncertainties from both quantities are correlated, e.g. a positive variation of $\log g$ of 0.1 dex needs to be compensated by an increase of T_{eff} ∼100-300 K to guarantee again the Si ionization balance. Although in many cases the formal errors in temperature obtained from the propagation of equivalent widths errors are smaller than 500 K, our experience warns us to be conservative (since other parameters can also slightly affect the derived temperatures, such as the considered microturbulence). Therefore, we adopt 500 K and 0.1 dex as characteristic uncertainties in T_{eff} and $\log g$, respectively, from our analyses.

3.5. Silicon and oxygen stellar abundances

We applied the curve of growth method to derive Si and O abundances. This method considers a grid of models for a given set of stellar parameters (T_{eff} and $\log g$) in which the microturbulence and the abundance of the element to be studied are varied. An abundance is obtained for the various values of microturbulence for each of the considered lines (given the measured *EW* of the lines in the observed spectrum). Then, the final abundance is given by that microturbulence which results in all lines giving the same abundance. More details on this method can be found in e.g. Kilian (1992) or Simón-Díaz et al. (2006).

Our motivation to prefer this methodology to perform the abundance analysis is that we find the curve of growth method very powerful to identify problematic lines (as it was shown e.g. in previous section) which can affect the final abundance determination, and provide precise estimations of the uncertainties associated with the dispersion of line-to-line abundances, microturbulence and the stellar parameters.

3.5.1. Silicon abundances

As mentioned in previous section, silicon abundance is obtained simultaneously to the stellar parameters. Once a first estimation of the stellar parameters was obtained through the EW(Si IV λ4116)/EW(Si III λ4552) and/or EW(Si II λ6371)/EW(Si III λ4552) line ratios, the curve of growth method was applied to a proper set of Si lines to derive the Si abundance together with the final values of the stellar parameters and a microturbulence.

Initially, we included all the measured lines in the analysis; however, we identified some problematic lines. By *problematic lines* we mean lines giving abundances too high or too low compared with the mean value provide by a set of lines initially considered as reliable; these problematic lines were removed in the final analysis. To illustrate the procedure, we consider the case of HD 36960. The ϵ_{Si}-EW diagram with whole set of measured Si lines (Si III and Si IV lines, in this case) is shown in Fig. 4. We consider as initial set of reliable lines the Si III $\lambda\lambda$4552, 4567, 4574 triplet and the Si IV λ4116 line. The other Si IV lines

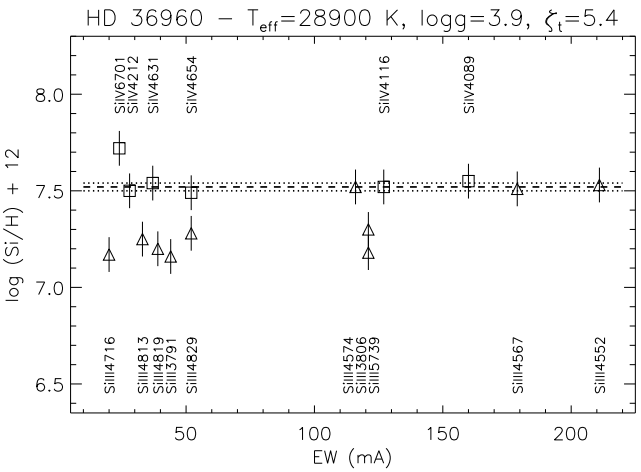

Fig. 4 Silicon abundance vs. equivalent width diagnostic diagrams for HD 36960. All the observed Si III-IV lines are included in the plot. uncertainties in the individual line abundances (propagated from the errors in the measured EWs) are indicated as vertical lines

provide similar abundances as the first set of reliable lines except Si IV λ6701. The situation is less encouraging for the other Si III lines, since all of them lie below the mean abundance value from reliable lines. We hence label these lines as problematic. Note that the same procedure was followed for the selection of reliable Si II lines (see Sect. 3.4).

A similar behavior is found for the problematic lines in all the analyzed stars. Since the equivalent width of these lines are accurately measured and no lines from other elements are expected to be affecting them[7], we argue that the discrepancy may be related with the definition of the model atom. For example, the Si III $\lambda\lambda$4813, 4819, 4829 triplet is known to give different results than the Si III $\lambda\lambda$4552, 4567, 4574 triplet due to boundary problems of the Si III model atom (Becker & Butler, 1990). Normally, there is a reason to explain the bad behavior of the problematic lines; therefore, the exclusion of lines from the analysis is not arbitrary (e.g. lines from the same multiplets behave in the same way and are normally excluded all together).

It is important to notice that the analysis with the whole set of lines (including the problematic ones) could led to an incorrect determination of the microturbulence, and hence the final value of Si abundance.

Final results of the Si abundance analysis[8] are indicated in Table 3 (columns 9 and 10). Three sources of errors must be considered for the estimation of the final uncertainty: (1) the dispersion in the line-by-line abundances, (2) the uncertainty associated with the microturbulence, (indicated in Table 3, and Tables 6-18, only available in the electronic version), and (3)

[7] This is not the case of Si IV $\lambda\lambda$4089, 4631, and Si II $\lambda\lambda$6347, 3856; these lines may be blended with O II λ4089, N II λ4631, Mg II λ6347, and O IIλ3856, respectively, in some cases. The high resolution of the FIES@NOTspectra normally allows to separate both line contributions; however, results obtained with these lines are always treated with care.

[8] Results of the line-by-line analysis are presented in Tables 6-18 (only available in the electronic version).

the contribution of uncertainties in the stellar parameters. These can be added quadratically to obtain the total uncertainty.

For illustrative purposes, we indicate in last column of Table 3 the effect of a change of ±500 K in T_{eff} on the Si abundance if this would be derived exclusively by using Si III lines[9]. The minimum effect occurs for $T_{eff} \sim 27000$ K and increases towards higher and lower temperatures (note the change in the sign of the uncertainties), reaching values up to 0.12 dex. This behavior is a consequence of the dependence of the equivalent width of the Si III lines with temperature; the maximum EW is achieved around 27000 K (and hence the abundance is quite insensible to changes small changes in T_{eff}), and decreases towards lower and higher temperatures (increasing also its sensibility to T_{eff} variations). When lines from two different ions are used, the final Si abundance can be constrained with a better accuracy, since the EW of lines from different ions behaves in a opposite way for a given T_{eff}. As a consequence, in this case the uncertainty associated with the stellar parameters is always negligible compared with the dispersion in the line-by-line abundances.

3.5.2. Oxygen abundances

Up to 47 O II lines were identified in the observed spectral range. However, not all the lines were finally used for the O abundance determination. The selection of the final set of lines used for the analysis was based on a detailed analysis by multiplets (following similar criteria than in the case of Si, but in this case we studied the behavior of lines resulting from different multiplets). We found a similar behavior of lines as the one described in Simón-Díaz et al. (2006).

The derived O abundances are indicated in Table 4, and the results of the line-by-line analyses in Tables 6-18 (in the electronic version). For this element, only lines from one ionization state were available, so we could not test if the corresponding ionization equilibrium (O III/II or O II/I) is achieved for the considered stellar parameters. We adopt for the oxygen abundance analysis the same stellar parameters as in the Si analysis.

We found (as in many other previous works) that the microturbulence derived from the O II lines (ξ_t(O)) differs from that resulting from the Si analysis (ξ_t(Si)); a somewhat larger microturbulence is derived. Some authors assume the ξ_t(Si) value (or a mean value of the microturbulences obtained for the various elements analyzed) to perform the oxygen abundance analysis. In our opinion, this can lead to important systematic errors in the analysis. Since this is an ad-hoc parameter still not well understood (see, however, Cantiello et al., 2009), we adopt the microturbulence derived from the oxygen analysis itself, for consistency.

In fact, the determination of the microturbulence value which will be adopted in the final steps of the abundance determination is an important task. Not identified problems in the O II line modeling or bad measurements of the corresponding equivalent widths (due to blends, noise, or a bad placement of the continuum), can enormously affect the ξ_t value which produce a zero slope in the ϵ_O-EW diagrams. A detailed analysis by multiplets (see Simón-Díaz, 2005) can help to identify problematic lines and to better decide the final microturbulence to be adopted.

Table 4 also indicates the uncertainties associated with errors in the line-to-line abundance dispersion, the microturbulence and the stellar parameters. In addition, last column show the derived abundances if the effective temperature is varied ±500 K. (Although the exact values are not shown here, the contribution of the log g uncertainty on the oxygen abundance can be considered negligible in comparison with the T_{eff} contribution.) Note that the derived oxygen abundance is very sensitive to changes in T_{eff} for the cooler and hotter objects, and that there is a change in the behavior of the oxygen abundance with T_{eff} around 27000 K. Note that this behavior is similar to the one illustrated in Table 3.

4. Comparison with previous works

Two of the stars included in this analysis were already analyzed in Simón-Díaz et al. (2006). These are HD 37020 and HD 37042. Note that we re-observed the two stars to have spectra with the same characteristics as the other stars in the sample. The stellar parameters presented in Table 2 correspond to the analysis of the new spectra. The new analysis resulted in slightly higher effective temperatures (but within the errors) and gravities $\sim 0.1-0.2$ dex larger. Several factors produced this difference in the derived stellar parameters. Firstly, in this paper we based our T_{eff} - log g determination on the HSi analysis, instead of using the H and He I-II lines. The best T_{eff} - log g pair reproducing simultaneously the Si III-IV ionization equilibrium and the wings of the H lines is the one indicated in Table 3. A lower log g requested an effective temperature somewhat lower (which was not fitting the He II lines). In addition, the better quality of the new spectra allowed us to better constraint the gravity of the stars. Note that the wings of the H lines are not very sensitive to changes of the order of $\sim$0.1-0.2 dex in log g in this range of stellar parameters. In Simón-Díaz et al., we based our criterium to decide the best final solution in the faint He II λ4541 line; however, it is better to rely on the HSi criterium, which is more sensitive in this range of stellar parameters. In fact, we have found that the new T_{eff}, - log g pair also fit nicely the He I-II lines. We hence prefer this last solution.

We also obtain ~0.05-0.10 dex higher oxygen abundances. Part of this difference is caused by the change of stellar parameters; in addition, we measured sligthly larger EWs for the O II lines in both stars. Note, however, that the old and new abundances are in agreement taking into account the error bars. The discrepancy found for these two objects between Simón-Díaz et al. (2006) and these new study serves as an example to illustrate the effect of intrinsic uncertainties in the determination of stellar abundances; the same author, following a similar methodology can find slightly different results (but within the errors) when analyzing spectra from two

[9] A similar test assuming a change of 0.1 dex in log g indicates negligible effects when compared with the T_{eff} contribution.

Table 4 Final results of the O abundance analysis. Detailed results (line-by-line) of the O abundance analysis are presented in Tables 6 to 18 in the electronic version of the paper.

Target	SpT	T_{eff}	log g	ξ_t(O)	ϵ_O	$\Delta\epsilon_O(\sigma)$	$\Delta\epsilon_O(\xi_t)$	$\Delta\epsilon_O(T_{eff}\pm500)$	$\epsilon_O(T_{eff}+500, T_{eff}-500)$
HD 36512	B0 V	33700	4.2	4.4±1.5	**8.71**	0.10	0.05	±0.06	(8.76, 8.65)
HD 37020	B0.5 V	30500	4.2	6.4±1.6	**8.70**	0.10	0.07	±0.05	(8.74, 8.65)
HD 36960	B0.5 V	28900	3.9	5.9±0.8	**8.71**	0.10	0.04	±0.03	(8.74, 8.68)
HD 37042	B0.7 V	29700	4.2	4.9±1.1	**8.75**	0.08	0.06	±0.02	(8.78, 8.74)
HD 36591	B1 V	27200	4.1	4.5±0.3	**8.71**	0.10	0.02	∓0.02	(8.71, 8.74)
HD 36959	B1 V	25800	4.2	2.1±0.4	**8.70**	0.06	0.02	∓0.05	(8.66, 8.76)
HD 37744	B1.5 V	23800	4.1	3.6±1.4	**8.70**	0.07	0.06	∓0.09	(8.61, 8.79)
HD 35299	B1.5 V	23700	4.2	2.8±0.6	**8.72**	0.07	0.03	∓0.09	(8.64, 8.82)
HD 36285	B2 V	20600	4.0	5.5±1.5	**8.80**	0.10	0.06	∓0.13	(8.67, 8.92)
HD 35039	B2 V	19800	3.7	5.3±1.5	**8.79**	0.07	0.07	∓0.15	(8.65, 8.94)
HD 36629	B2 V	20000	4.1	6.0±1.7	**8.76**	0.10	0.06	∓0.14	(8.62, 8.89)
HD 36430	B2 V	18600	4.1	6.3±2.2	**8.76**	0.07	0.08	∓0.13	(8.64, 8.90)
HD 35912	B2 V	18500	4.0	6.3±2.2	**8.79**	0.09	0.08	∓0.13	(8.67, 8.93)

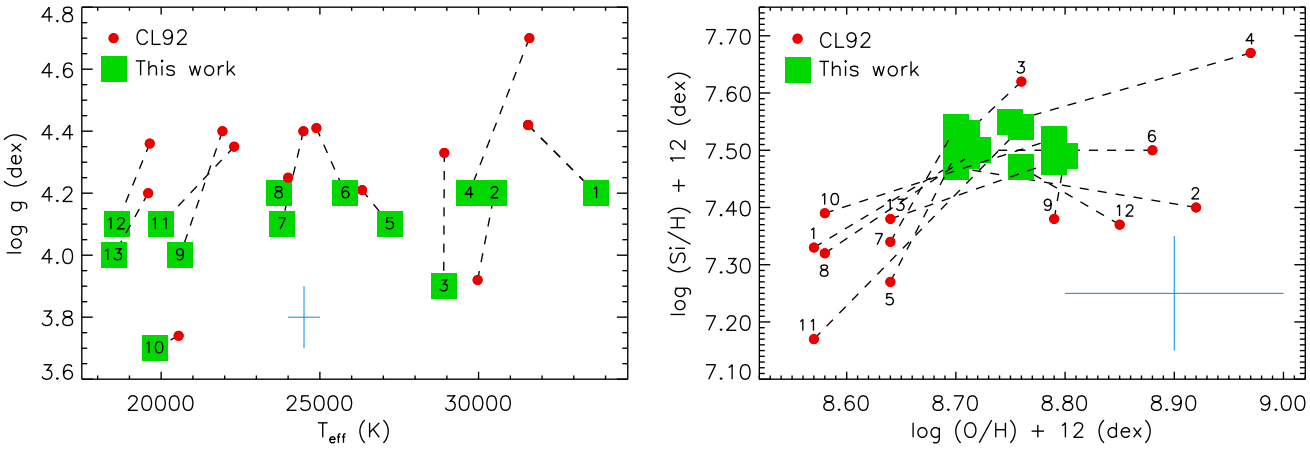

Fig. 5 Comparison of our derived stellar parameters, Si and O abundances with those obtained by Cunha & Lambert (1992, 1994). Results from both studies for each star are connected with a dashed line. Numbers follow the order of stars presented in Tables 3 and 4. The size of the uncertainties of the various quantities are shown by the crosses.

different observational campaigns[10].

Recently, Przybilla, Nieva, & Butler (2008) analyzed a representative sample of unevolved early B-type stars in nearby OB associations and the field using a similar technique but a different stellar atmosphere code (line blanketed ATLAS9 LTE model atmospheres, Kurucz 1993), and NLTE line-formation calculations (performed using updated versions of DETAIL and SURFACE, Giddings 1981; Butler & Giddings 1985). They have one star in common with our work, HD 36591 (HR 1861). We obtain very similar results for the stellar parameters, as well as the Si and O abundances. Note that they used several T_{eff} spectroscopic indicators (apart from Si II-IV), finding a very good overall agreement.

Gummersbach et al. (1998) included a sample of 5 stars from Ori OB1 in their study of the abundance gradient of the Galaxy. We have three stars in common. Gummersbach et al. used a self-consistent spectroscopic approach. We find similar effective temperatures for the two hotter objects (when Si IV lines are available), but ∼0.2 dex lower gravities. For these stars (HD 36959 and HD 36960) the derived Si and O abundances are in agreement (within the errors) with our values. The difference in gravity could explain their slightly lower O abundances.

Interestingly, for the cooler object in common (HD 35039) we obtain lower T_{eff} and log g. It is remarkable that they obtained very low O and Si abundances (8.20 and 7.08 dex, respectively) for this star. Probably, this result is related with the Si II problem we described in Sect. 3.4 (see also lower pannel in Fig. 2); they used line Si II 4130 to establish T_{eff}, and hence obtained a too high value (23500 K vs. 19900 K, the value we obtained). For this range of stellar parameters, higher T_{eff} supposes lower O abundances; a change of ∼3000 K in T_{eff} can perfectly explain a 0.5 dex variation of the O abundance.

Figure 5 presents a comparison our results with those obtained by Cunha & Lambert (1992, 1994) concerning the stellar parameters, Si and O abundances. There is a clear discrep-

[10] The different results may be also caused by actual changes in the stellar spectra (e.g. due to binarity).

ancy for the majority of the objects, not only in terms of effective temperatures, but also gravities. Cunha & Lambert (1992, 1994) made use of the calibrations of Strömgen photometry coupled with the fits to the pressure-broadened line wings of Hγ (from Kurucz, 1979, LTE stellar atmopsheres) in order to derive $T_{\rm eff}$ and $\log g$. Following Gies & Lambert (1992) they adjusted upward by 4.2% and 5.2% the $T_{\rm eff}$ calibrations by Lester et al. (1986) and Balona (1984), respectively. The discrepancy in effective temperatures obtained through commonly used photometric calibrations and spectroscopic line diagnostic has already pointed out by several authors (e.g. Kilian et al., 1991; Nieva & Przybilla, 2008). Our result remarks once more these discrepancies.

Note also the large discrepancy found for the gravity. Cunha & Lambert values are systematically larger (~0.3 dex). As shown by Nieva & Przybilla (2007) the use of LTE profiles for the gravity determination lead to overestimated $\log g$ values, in particular for hotter stars. In figure 3 we show a comparison of synthetic hydrogen lines from two FASTWIND models with the observed profiles for HD 36960 (labeled with #3 in Fig. 5. One of the models considers the stellar parameters derived from our analysis, the other one correspond to the $T_{\rm eff}$-$\log g$ pair provided by Cunha & Lambert (1992). The difference in the wings of the lines is clear.

We also find important discrepancies in the derived Si and O abundance for most of the stars, with a no systematic trend (i.e. differences are found in both positive and negative directions). There are several factors which must be taken into account to explain this disagreement. One of them is the imprecise determination of the stellar parameters from photometric indexes. But maybe the most important one is the following. Once the stellar parameters were calculated as described above, Cunha & Lambert used those values to perform the abundance analysis, computing line-blanketed LTE model atmospheres with ATLAS6 (Kurucz, 1979) for the LTE case, or using a grid of *EW*s based on Gold's models (Gold, 1984) for the NLTE abundance calculations. The risk of this strategy is that the stellar abundance analysis is decoupled of the stellar parameters determination, and this could produce inconsistencies in the analysis process. Briefly, the calculation of *EW*s of the lines used for the abundance determination is based on the stellar atmosphere structure defined by a stellar atmosphere model computed for the given set of stellar parameters; on the other hand, the stellar parameters derived for a given star will depend on the characteristics of the stellar atmosphere model we have used[11]. Therefore, it may be dangerous to do an abundance analysis with a certain stellar atmosphere code using the stellar parameters obtained from a different code or a photometric calibration. This argument is crucial in the case of stars with $T_{\rm eff} \geq 30000$ K, where photometric methods become completely unreliable discriminators of temperatures and gravities, due to the insensitivity of the Rayleigh-Jeans tail of the spectral energy distribution on temperature.

A self-consistent spectroscopic approach allows to minimize this problem. In this case, the stellar parameters are determined by fitting certain spectroscopic diagnostics and then the same models are used for the abundance analysis. This way we are sure that the stellar atmosphere structure used for the computation of the abundance diagnostics is coherent with the derived stellar parameters for the studied star. To a first order, when the whole analysis is performed with stellar atmosphere codes with different characteristics the derived abundances should be quite similar (although the derived stellar parameters could be somewhat different). This approach can be strengthened if multiple independent spectroscopic indicators are considered (i.e. Si III-IV, He I-II, C II-IV; see e.g. this study or Nieva & Przybilla, 2008).

5. Chemical composition of B-type stars in the Ori OB1 association

Figures 6 and 7 show again the derived oxygen and silicon abundances in our sample of B-type stars in the Ori OB1 association, along with the results by Cunha & Lambert (1994). This time, the stars are ordered following the subgroups suggested by Blaauw (1964). As commented in Cunha & Lambert (1994), they found that the stars in the youngest group (Id) and some of the stars in subgroup Ic were enriched in oxygen by about 40% relative to the stars belonging to the older subgroups. They interpreted this result as a possible proof of enrichment of the new generation of stars in the association with the resulted products from supernovae ejecta from the older subgroups. In addition, they found features of this enrichment in silicon (also expected from the triggered star formation scenario). Contrarily, we did not find any systematic difference between the O and Si abundances in stars from the various associations. In fact, our results indicate that the B-type stars in the Ori OB1 association are chemically homogeneous (at least in terms of oxygen and silicon), having a dispersion in abundances (0.04 and 0.03 dex, respectively; marked as horizontal dashed lines) smaller than the intrinsic uncertainties of the derived abundances (0.10 and 0.08 dex, respectively, marked as horizontal dash-dotted lines). The mean abundances are ϵ(O) = 8.73 dex and ϵ(Si) = 7.51 dex. These values are in agreement with those obtained by Przybilla, Nieva, & Butler (2008) for their sample of six stars in the solar neighborhood.

5.1. Comparison with the Sun

We also include in Figure 6 the resulting solar oxygen abundances appeared in the literature in the last 4 years (during the so called solar oxygen crisis[12] epoch, not yet finished). Various authors published values for the solar oxygen abundance based on improved model atmospheres (either 1D and 3D), line formation codes, atomic and molecular data, and detailed treatment of blends. In the plot, we present results by Centeno & Socas-Navarro (2008); Meléndez & Asplund (2008); Ayres

[11] As an example, we want to mention the consequences that the inclusion of the line blanketing and wind blanketing effects in the stellar atmosphere models of O and early B-type stars had on the SpT - $T_{\rm eff}$ calibrations of these stars (see e.g. Martins et al., 2005; Repolust, Puls, & Herrero, 2004).

[12] Ayres et al. (2006)

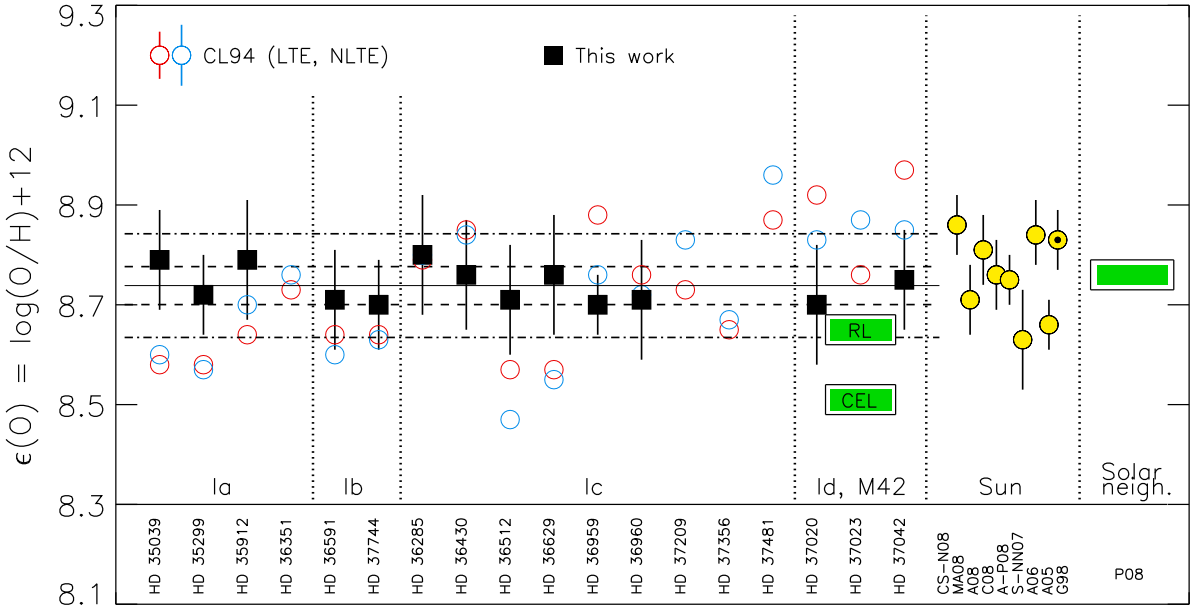

Fig. 6 Oxygen abundances derived for our sample of early B-type stars in the Orion association, and comparison with the previous results from Cunha & Lambert (1994). Vertical lines separates stars from the various subgroups. Solid and dashed horizontal lines represents the mean value and the dispersion (1σ) of our results; dot-dashed horizontal lines indicate the characteristic intrinsic uncertainty of the derived abundances (accounting for uncertainties in stellar parameters, microturbulence, and the line-by-line abundance dispersion). The oxygen abundance derived by Esteban et al. (2004) for M 42, along with the values determined for the Solar abundance in the last 4 years (the epoch of the "solar crisis"), are also presented for comparison.

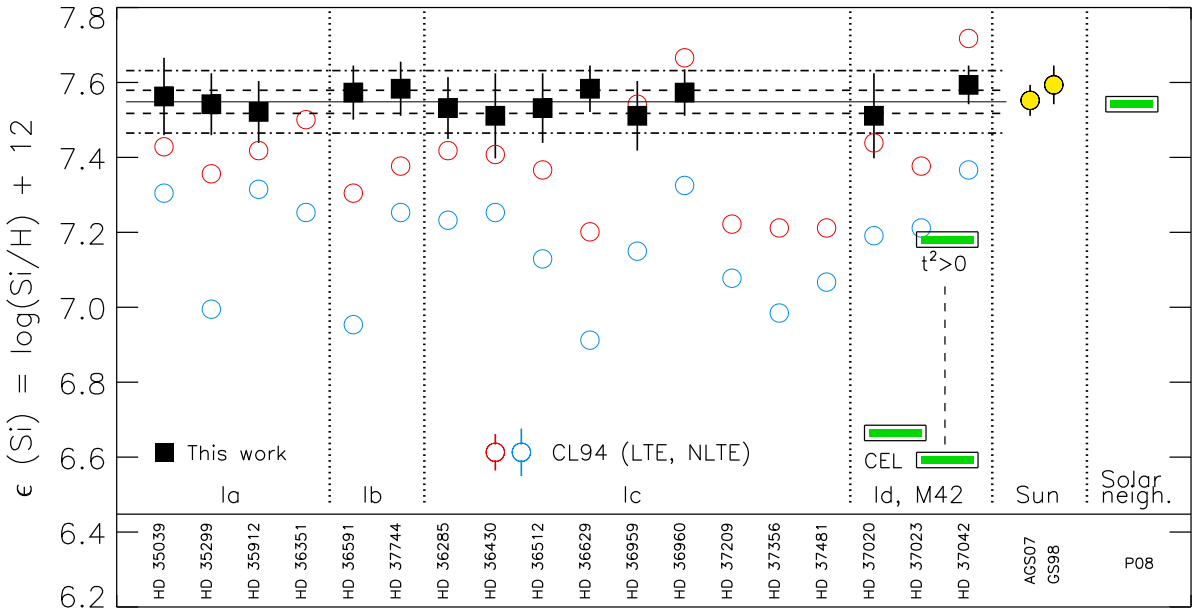

Fig. 7 As Fig. 2 but for silicon. This time, the reference for the nebular abundance is Rubin et al. (1993) and Garnett et al. (1995) (first and second column, see text). Solar values from Asplund, Grevesse, & Sauval (2005) and Grevesse & Sauval (1998)

(2008); Caffau et al. (2008); Allende Prieto (2008); Socas-Navarro & Norton (2007); Ayres et al. (2006); Asplund et al. (2004), and Grevesse & Sauval (1998). This last value (marked with a internal black dot) was considered as the standard solar O abundance until a few years ago. The derived solar values range from 8.63 dex (Socas-Navarro & Norton, 2007) to 8.86 dex (Centeno & Socas-Navarro, 2008). The O abundances in our sample of stars in Ori OB1 lay in the middle of all these values. In view of the present-day results the only thing we can say is that oxygen abundances in the Sun and B-type stars in the solar vicinity are the same within the uncertainties. However, we consider too premature to launch any firm conclusion or hypothesis about the chemical evolution of the local interstellar medium during the lifetime of the Sun.

Figure 7 also shows a comparison of our derived Si abundances with the Solar value. We only present here the old abun-

dance (Grevesse & Sauval, 1998) and the new value proposed by Asplund, Grevesse, & Sauval (2005). Contrarily to previous results, the mean Si abundance in B-type stars in Ori OB1 is very close to the Solar value (similarly to other B-type stars in the solar vicinity Przybilla, Nieva, & Butler, 2008).

5.2. Comparison with the Orion nebula

The most recent and detailed analysis of the optical spectrum of the Orion nebula was done by Esteban et al. (2004). The high quality UVES@VLT spectrum they used allowed them to derive the oxygen gas phase abundance of the nebula by using collisionally excited lines (CELs) and recombination lines (RLs). The final value they proposed is 8.65±0.03 dex. This value was calculated assuming the ionic abundances given by O^{2+} RLs and O^{+} CEL (plus a t^2=0.022)[13]. Note, however, that the abundance given by the O^{2+} and O^{+} CELs (and t^2=0) is 8.51±0.03 dex. These values have been included in Fig. 6 for comparison with the early B-type stellar abundances presented in this study. The mean value of the derived stellar oxygen abundances is 0.25 and 0.11 dex higher than the nebular abundances given by the CELs and RLs, respectively.

Although the mean stellar abundance seems to agree better with that given by the faint recombination lines, we have to take into account that the analysis of the nebular emission line spectrum can only provide us abundances for the ionized gas phase of the ISM. This means a lower limit of the actual ISM abundance, since part of the oxygen can be depleted, forming part of dust grains.

Silicon is one of the elements expected to be more depleted onto dust grains, along with Mg and Fe (Draine, 2003). We can hence compare our derived Si abundances with those obtained from the study of the emission line spectrum of the Orion nebula to try to find some clues about the amount of oxygen depleted. One should note that the determination of Si nebular abundances is not straightforward and must be based on results from photoionization models and certain ionization correction factors (ICFs). The only determinations of Si abundance in the Orion nebula we found in the literature are those by Rubin et al. (1993) and Garnett et al. (1995). Both studies used the same observations of the FUV Si III] $\lambda\lambda$1883, 1892 and C III] $\lambda\lambda$1907, 1909 lines to estimate the Si abundance, and obtained 6.65 and 6.58 dex, respectively. They computed photoionization models to obtain Si/H (Rubin et al., 1993) and the ICF necessary to transform Si^{2+}/C^{2+} into Si/C, and hence the C/O and O/H ratios to derive Si/H (Garnett et al., 1995). In addition, Garnett et al. (1995) discuss about how the effect of assuming a t^2=0.04 (Peimbert et al., 1993) in the calculation of the C/O and O/H ratios could affect the derived Si abundance. They obtained for this case log (Si/H)+12 = 7.14 dex. These three values of the Si abundance are included in Fig 7 for comparison with the stellar abundances. The difference between stellar and gas phase Si abundances are ∼1 dex, or ∼0.3 dex, depending of the nebular abundances we trust more.

Since a detailed comparison of stellar and nebular abundances in Ori OB1 and the Orion nebula within a dust-depletion scenario requires a more extended study, which is out of the scope of this paper, we decide to present a more detailed discussion in a separate paper (in preparation).

6. Summary and conclusion

In this work, we applied a self-consistent spectroscopic approach for the determination of the stellar parameters, Si and O abundances of a sample of early-B type stars from the various subgroups of the Ori OB1 association. We made use of a high-quality spectroscopic data-set, obtained with FIES@NOT, and the modern NLTE, line blanketed, spherically extended stellar atmosphere code FASTWIND.

We developed several IDL programs to automatically identify and measure the equivalent width of metal lines in high-resolution spectra. We also constructed a grid of FASTWIND HHeSiO models optimized for the analysis of early B-type, main sequence stars.

The availability of a large number of Si II-III-IV lines in the FIES@NOT spectra allowed us to obtain the stellar parameters with high accuracy and detect some problems related with some Si lines commonly used for the stellar parameter and Si abundance determination. Once these problems are accounted for, a high degree of homogeneity is found for Si abundances in the analyzed sample of stars.

The oxygen abundance analysis also result in a small dispersion of abundances, contrarily to previous determinations.

The mean oxygen and silicon abundances agree with those resulting from a similar analysis of a representative sample of unevolved early B-type stars in the solar vicinity (Przybilla, Nieva, & Butler, 2008). Both results indicate that abundances derived from these stellar objects are more homogeneous and metal rich than previously though.

We also compared the O and Si stellar abundance in Ori OB1 with those obtained for the Sun during the epoch of the "Solar crisis". The O abundances in our sample of stars in Ori OB1 lay in the middle of all these values. In view of the present-day results the only thing we can say is that oxygen abundances in the Sun and B-type stars in the solar vicinity are the same within the uncertainties. However, we consider too premature to launch any firm conclusion or hypothesis about the chemical evolution of the local interstellar medium during the lifetime of the Sun. Silicon abundances are also very similar (contrarily to what was previously found from the study of B-type stars).

Finally, we compared the stellar abundances with those derived from the study of the emission line spectrum of the Orion nebula. In a forthcoming paper we will present a more detailed discussion accounting for the possible depletion of O, Si, Mg and Fe into dust.

This work remarks one more time the importance of self-consistent spectroscopic abundance analyses for the determination of the chemical composition of the photospheres of OB-type stars. Photometric $T_{\rm eff}$ diagnostics must be treated with

[13] The t^2 parameter was introduced by Peimbert (1967) to account for the presence of temperature fluctuations in ionized nebulae. The temperature fluctuation scenario has been proposed to explain the CELs vs. RL abundance discrepancy (see García-Rojas & Esteban, 2007, and references therein).

caution in the context of abundance analyses of these type of objects. It is also dangerous to combine the stellar parameters determined with a certain code and the abundance analysis performed with a different code. Systematic errors inherent to those techniques, or possible biases between the various codes can lead to wrong abundances.

Acknowledgements. Financial support by the Spanish Ministerio de Ciencia e Innovación under the project AYA2008-06166-C03-01. This work has also been partially funded by the Spanish MICINN under the Consolider-Ingenio 2010 Program grant CSD2006-00070: First Science with the GTC (http://www.iac.es/consolider-ingenio-gtc). I'm really grateful with A. Herrero (Spain), G. Stasinska (France), and D. Schaerer (Switzerland) for their support and hospitality during the development of this work. I also acknowledge A. Herrero, M. Urbaneja, D. Lennon, F. Najarro, C. Trundle, and N. Castro for fruitful discussions. J. Puls, N. Przybilla, F. Nieva, and M. Urbaneja for the careful reading of the first version of this paper and all their comments. Finally, J. Puls for allowing me to use the stellar atmosphere code FASTWIND.

References

Allende Prieto, C. 2008, 14th Cambridge Workshop on Cool Stars, Stellar Systems, and the Sun, 384, 39
Asplund, M., Grevesse, N., Sauval, A. J., Allende Prieto, C., & Kiselman, D. 2004, A&A, 417, 751
Asplund M., Grevesse N., Sauval A. J., 2005, ASPC, 336, 25
Ayres, T. R., Plymate, C., & Keller, C. U. 2006, ApJS, 165, 618
Ayres, T. R. 2008, ApJ, 686, 731
Balona, L. A. 1984, MNRAS, 211, 973
Becker, S. R., & Butler, K. 1988, A&A, 201, 232
Becker S. R., Butler K., 1990, A&A, 235, 326
Blaauw, A. 1964, ARA&A, 2, 213
Briceño C., Calvet N., Hernández J., Vivas A. K., Hartmann L., Downes J. J., Berlind P., 2005, AJ, 129, 907
Brown, A. G. A., de Geus, E. J., & de Zeeuw, P. T. 1994, A&A, 289, 101
Caffau, E., Ludwig, H.-G., Steffen, M., Ayres, T. R., Bonifacio, P., Cayrel, R., Freytag, B., & Plez, B. 2008, A&A, 488, 1031
Cantiello M., et al., 2009, A&A, 499, 279
Cartledge S. I. B., Lauroesch J. T., Meyer D. M., Sofia U. J., 2006, ApJ, 641, 327
Carigi L., Peimbert M., Esteban C., García-Rojas J., 2005, ApJ, 623, 213
Centeno, R., & Socas-Navarro, H. 2008, ApJ, 682, L61
Chiappini C., Romano D., Matteucci F., 2003, MNRAS, 339, 63
Cowie, L. L., Songaila, A., & York, D. G. 1979, ApJ, 230, 469
Crowther, P. A., Lennon, D. J., & Walborn, N. R. 2006, A&A, 446, 279
Cunha, K., & Lambert, D. L. 1992, ApJ, 399, 586
Cunha, K., & Lambert, D. L. 1994, ApJ, 426, 170
Draine, B. T. 2003, ARA&A, 41, 241
Esteban, C., Peimbert, M., García-Rojas, J., Ruiz, M. T., Peimbert, A., & Rodríguez, M. 2004, MNRAS, 355, 229
García-Rojas, J., & Esteban, C. 2007, ApJ, 670, 457
Garnett, D. R., Dufour, R. J., Peimbert, M., Torres-Peimbert, S., Shields, G. A., Skillman, E. D., Terlevich, E., & Terlevich, R. J. 1995, ApJ, 449, L77
Gies, D. R., & Lambert, D. L. 1992, ApJ, 387, 673
Gray D. F., 1976, *The Observation and analysis of Stellar Photospheres, 1st Edition, Cambridge University Press*
Gold, M. 1984, Diplomarbeit, Ludwig-Maximilians-Universität München
Grevesse, N., & Sauval, A. J. 1998, Space Science Reviews, 85, 161
Gummersbach C. A., Kaufer A., Schaefer D. R., Szeifert T., Wolf B., 1998, A&A, 338, 881
Herrero, A., Kudritzki, R. P., Vilchez, J. M., Kunze, D., Butler, K., & Haser, S. 1992, A&A, 261, 209
Herrero A., Lennon D. J., 2004, IAUS, 215, 209
Kilian, J., Becker, S. R., Gehren, T., & Nissen, P. E. 1991, A&A, 244, 419
Kilian, J. 1992, A&A, 262, 171
Kurucz, R. L. 1979, ApJS, 40, 1
Lester, J. B., Gray, R. O., & Kurucz, R. L. 1986, ApJS, 61, 509
Martins, F., Schaerer, D., & Hillier, D. J. 2005, A&A, 436, 1049
Markova, N., & Puls, J. 2008, A&A, 478, 823
Meyer D. M., Jura M., Cardelli J. A., 1998, ApJ, 493, 222
Meléndez J., Asplund M., 2008, A&A, 490, 817
Morel T., 2009, CoAst, 158, 122
Nieva M.-F., & Przybilla N., 2007, A&A, 467, 295
Nieva, M.-F., & Przybilla, N. 2008, A&A, 481, 199
Nieva M.-F., Przybilla N., 2009, arXiv, arXiv:0902.2949
Peimbert M., 1967, ApJ, 150, 825
Peimbert, M., Storey, P. J., & Torres-Peimbert, S. 1993, ApJ, 414, 626
Przybilla N., Nieva M.-F., Butler K., 2008, ApJ, 688, L103
Puls, J., Urbaneja, M. A., Venero, R., Repolust, T., Springmann, U., Jokuthy, A., & Mokiem, M. R. 2005, A&A, 435, 669
Repolust T., Puls J., Herrero A., 2004, A&A, 415, 349
Reynolds, R. J., & Ogden, P. M. 1979, ApJ, 229, 942
Rubin, R. H., Dufour, R. J., & Walter, D. K. 1993, ApJ, 413, 242
Santolaya-Rey, A. E., Puls, J., & Herrero, A. 1997, A&A, 323, 488
Simón-Díaz, S., 2005, thesis, Univ. de La Laguna, Spain.
Simón-Díaz, S., Herrero, A., Esteban, C., & Najarro, F. 2006, A&A, 448, 351
Simón-Díaz S., Herrero A., 2007, A&A, 468, 1063
Socas-Navarro, H., & Norton, A. A. 2007, ApJ, 660, L153
Trundle C., Lennon D. J., Puls J., Dufton P. L., 2004, A&A, 417, 217
Urbaneja, M. A., Herrero, A., Kudritzki, R.-P., Najarro, F., Smartt, S. J., Puls, J., Lennon, D. J., & Corral, L. J. 2005, ApJ, 635, 311

Online Material

Table 5 List of $\log gf$ values for the Si II-IV lines considered in this study (from Atomic Line List v2.05). For the O II lines we refer to Simón-Díaz et al. (2006)

Ion	λ Å	$\log gf$	Configuration	Term
Si II	3856.02	-0.4569	3s $3p^2$-$3s^2$ (1S) 4p	2D-2Po
Si II	3862.60	-0.7130	3s $3p^2$-$3s^2$ (1S) 4p	2D-2Po
Si II	4128.10	0.3646	$3s^2$ (1S) 3d-$3s^2$ (1S) 4f	2D-2Fo
Si II	4130.90	0.5192	$3s^2$ (1S) 3d-$3s^2$ (1S) 4f	2D-2Fo
Si II	5041.02	0.2543	$3s^2$ (1S) 4p-$3s^2$ (1S) 4d	2Po-2D
Si II	5055.98	0.5083	$3s^2$ (1S) 4p-$3s^2$ (1S) 4d	2Po-2D
Si II	5056.32	-0.4460	$3s^2$ (1S) 4p-$3s^2$ (1S) 4d	2Po-2D
Si II	6347.11	0.1819	$3s^2$ (1S) 4s-$3s^2$ (1S) 4p	2S-2Po
Si II	6371.37	-0.1208	$3s^2$ (1S) 4s-$3s^2$ (1S) 4p	2S-2Po
Si III	4552.62	0.2828	3s 4s-3s 4p	3S-3Po
Si III	4567.84	0.0595	3s 4s-3s 4p	3S-3Po
Si III	4574.76	-0.4183	3s 4s-3s 4p	3S-3Po
Si III	5739.73	-0.1032	3s 4s-3s 4p	1S-1Po
Si IV	4088.86	0.1984	$2p^6$ 4s-$2p^6$ 4p	2S-2Po
Si IV	4116.10	-0.1055	$2p^6$ 4s-$2p^6$ 4p	2S-2Po
Si IV	4212.40	0.3840	$2p^6$ 5d-$2p^6$ 6f	2D-2Fo
Si IV	4212.41	0.5601	$2p^6$ 5d-$2p^6$ 6f	2D-2Fo
Si IV	4631.24	1.2158	$2p^6$ 5f-$2p^6$ 6g	2Fo-2G

Table 6 Results from the abundance analysis of HD 36512 (B0 V)

HD 36512	$T_{\rm eff}$ = 33700 K, log g = 4.2 dex			$\xi_{\rm t}$(Si)=4.3
Line	EW (mÅ)	ΔEW (mÅ)	$\epsilon_{\rm Si}$ (dex)	$\Delta\epsilon_{\rm Si}$ (dex)
SiIII4552	117	4	7.51	0.07
SiIII4567	99	5	7.58	0.08
SiIII4574	50	4	7.53	0.09
SiIV4089	189	5	7.42	0.06
SiIV4116	166	5	7.54	0.07
SiIV4212	53	3	7.46	0.06
SiIV4631	75	4	7.40	0.06
			$\epsilon_{\rm Si}$ = **7.49**	$\Delta\epsilon_{\rm Si}(\sigma)$ = 0.07
	$\Delta\xi_{\rm t}$(Si) = 0.7		⇒	$\Delta\epsilon_{\rm Si}(\xi_{\rm t})$ = 0.05

HD 36512	$T_{\rm eff}$ = 33700 K, log g = 4.2 dex			$\xi_{\rm t}$(O)=4.4
Line	EW (mÅ)	ΔEW (mÅ)	$\epsilon_{\rm O}$ (dex)	$\Delta\epsilon_{\rm O}$ (dex)
OII3945	36	5	8.81	0.13
OII3954	63	5	8.86	0.09
OII3982	29	5	8.63	0.14
OII4317	78	11	8.74	0.16
OII4319	75	5	8.77	0.08
OII4366	70	8	8.70	0.14
OII4414	89	6	8.55	0.09
OII4416	76	9	8.66	0.15
OII4452	25	10	8.59	0.33
OII4641	95	12	8.69	0.20
OII4661	82	4	8.88	0.07
OII4673	23	3	8.83	0.12
OII4676	61	5	8.67	0.10
OII4696	13	6	8.73	0.37
OII6721	30	8	8.71	0.20
OII4072	84	8	8.62	0.15
OII4076	101	6	8.64	0.11
OII4078	33	6	8.73	0.18
OII4086	48	8	8.88	0.20
OII4089	77	6	8.63	0.10
OII4891	19	5	8.65	0.20
OII4906	34	5	8.67	0.13
OII4943	46	3	8.59	0.06
			$\epsilon_{\rm O}$ = **8.71**	$\Delta\epsilon_{\rm O}(\sigma)$ = 0.10
	$\Delta\xi_{\rm t}$(O) = 1.5		⇒	$\Delta\epsilon_{\rm O}(\xi_{\rm t})$ = 0.05

Table 7 Results from the abundance analysis of HD 37020 (B0.5 V)

HD 37020	$T_{\rm eff}$ = 30500 K, log g = 4.2 dex			$\xi_{\rm t}$(Si)=0.5
Line	EW (mÅ)	ΔEW (mÅ)	$\epsilon_{\rm Si}$ (dex)	$\Delta\epsilon_{\rm Si}$ (dex)
SiIII4552	130	13	7.56	0.27
SiIII4567	110	7	7.54	0.14
SiIII4574	74	9	7.57	0.22
SiIII5739	73	9	7.38	0.19
SiIV4089	104	21	7.29	0.42
SiIV4116	90	8	7.41	0.17
SiIV4212	25	5	7.43	0.21
SiIV4631	47	7	7.55	0.17
			$\epsilon_{\rm Si}$ = **7.47**	$\Delta\epsilon_{\rm Si}(\sigma)$ = 0.10
	$\Delta\xi_{\rm t}$(Si) = 0.5		⇒	$\Delta\epsilon_{\rm Si}(\xi_{\rm t})$ = 0.04

HD 37020	$T_{\rm eff}$ = 30500 K, log g = 4.2 dex			$\xi_{\rm t}$(O)=6.4
OII3945	56	10	8.75	0.19
OII3954	90	10	8.77	0.15
OII4317	94	10	8.56	0.13
OII4319	106	13	8.73	0.18
OII4366	104	13	8.71	0.19
OII4414	130	10	8.50	0.12
OII4416	119	10	8.68	0.13
OII4452	62	12	8.83	0.21
OII4638	101	10	8.83	0.15
OII4641	141	10	8.73	0.14
OII4661	105	10	8.71	0.15
OII4676	94	12	8.67	0.19
OII6721	61	12	8.77	0.19
OII4076	144	10	8.73	0.15
OII4891	40	8	8.84	0.19
OII4906	48	9	8.63	0.18
OII4941	48	6	8.57	0.12
OII4943	65	8	8.53	0.13
			$\epsilon_{\rm O}$ = **8.70**	$\Delta\epsilon_{\rm O}(\sigma)$ = 0.10
	$\Delta\xi_{\rm t}$(O) = 1.6		⇒	$\Delta\epsilon_{\rm O}(\xi_{\rm t})$ = 0.07

Table 8 Results from the abundance analysis of HD 36960 (B0.5 V)

HD 36960	T_{eff} = 28900 K, log g = 3.9 dex			ξ_t(Si)=5.4
Line	EW (mÅ)	ΔEW (mÅ)	ϵ_{Si} (dex)	$\Delta\epsilon_{Si}$ (dex)
SiIII4552	211	5	7.53	0.06
SiIII4567	179	5	7.51	0.06
SiIII4574	116	5	7.52	0.07
SiIV4089	160	11	7.55	0.15
SiIV4116	127	9	7.52	0.14
SiIV4212	28	4	7.50	0.14
SiIV4631	37	3	7.54	0.08
			ϵ_{Si} = **7.53**	$\Delta\epsilon_{Si}(\sigma) = 0.02$
	$\Delta\xi_t$(Si) = 0.6		⇒	$\Delta\epsilon_{Si}(\xi_t) = 0.06$

HD 36960	T_{eff} = 28900 K, log g = 3.9 dex			ξ_t(O)=5.9
OII3945	68	6	8.78	0.11
OII3954	96	7	8.71	0.10
OII3982	61	6	8.63	0.11
OII4317	125	7	8.71	0.08
OII4319	125	6	8.78	0.08
OII4366	113	5	8.66	0.07
OII4414	165	5	8.66	0.06
OII4416	141	5	8.75	0.06
OII4452	50	5	8.54	0.10
OII4661	127	5	8.87	0.08
OII4673	46	5	8.85	0.12
OII4676	101	5	8.66	0.08
OII4696	30	3	8.78	0.09
OII6641	47	6	8.81	0.12
OII6721	76	9	8.77	0.12
OII4078	60	4	8.81	0.09
OII4891	34	10	8.64	0.27
OII4906	61	6	8.71	0.11
OII4941	54	10	8.54	0.19
OII4943	75	4	8.54	0.06
OII4956	23	4	8.72	0.14
			ϵ_O = **8.71**	$\Delta\epsilon_O(\sigma) = 0.10$
	$\Delta\xi_t$(O) = 0.8		⇒	$\Delta\epsilon_O(\xi_t) = 0.04$

Table 9 Results from the abundance analysis of HD 37042 (B0.7 V)

HD 37042	T_{eff} = 29700 K, log g = 4.2 dex			ξ_t(Si)=1.4
Line	EW (mÅ)	ΔEW (mÅ)	ϵ_{Si} (dex)	$\Delta\epsilon_{Si}$ (dex)
SiIII4552	149	2	7.54	0.04
SiIII4567	133	6	7.59	0.11
SiIII4574	88	4	7.56	0.08
SiIII5739	99	7	7.50	0.13
SiIV4116	95	10	7.53	0.21
SiIV4212	24	5	7.54	0.22
SiIV4631	35	10	7.55	0.30
			ϵ_{Si} = **7.55**	$\Delta\epsilon_{Si}(\sigma) = 0.03$
	$\Delta\xi_t$(Si) = 0.3		⇒	$\Delta\epsilon_{Si}(\xi_t) = 0.04$

HD 37042	T_{eff} = 29700 K, log g = 4.2 dex			ξ_t(O)=4.9
OII3945	68	6	8.87	0.11
OII3954	93	7	8.79	0.12
OII4317	116	10	8.75	0.13
OII4319	116	11	8.84	0.16
OII4366	108	9	8.76	0.14
OII4414	143	10	8.64	0.13
OII4416	127	7	8.78	0.10
OII4452	64	6	8.82	0.12
OII4641	142	7	8.81	0.11
OII4661	108	5	8.79	0.09
OII4676	95	6	8.71	0.11
OII4696	30	5	8.82	0.16
OII4072	110	10	8.62	0.18
OII4076	128	10	8.63	0.17
OII4078	57	8	8.84	0.19
OII4891	39	5	8.80	0.13
OII4906	57	5	8.75	0.10
OII4941	53	4	8.63	0.08
OII4943	73	4	8.63	0.07
OII4956	23	8	8.79	0.29
			ϵ_O = **8.75**	$\Delta\epsilon_O(\sigma) = 0.08$
	$\Delta\xi_t$(O) = 1.1		⇒	$\Delta\epsilon_O(\xi_t) = 0.06$

Table 10 Results from the abundance analysis of HD 36591 (B1 V)

HD 36591	T_{eff} = 27200 K, log g = 4.1 dex			ξ_t(Si)=1.3
Line	EW (mÅ)	ΔEW (mÅ)	ϵ_{Si} (dex)	$\Delta\epsilon_{Si}$ (dex)
SiIII4552	158	2	7.52	0.03
SiIII4567	145	2	7.62	0.04
SiIII4574	104	2	7.65	0.04
SiIII5739	114	2	7.56	0.03
SiIV4089	80	2	7.54	0.05
SiIV4116	61	2	7.48	0.06
			ϵ_{Si} **= 7.53**	$\Delta\epsilon_{Si}(\sigma) = 0.06$
	$\Delta\xi_t$(Si) = 0.3		⇒	$\Delta\epsilon_{Si}(\xi_t) = 0.03$
HD 36591	T_{eff} = 27200 K, log g = 4.1 dex			ξ_t(O)=4.5
OII3945	69	2	8.80	0.04
OII3954	86	2	8.64	0.04
OII3982	62	2	8.64	0.04
OII4317	125	5	8.77	0.06
OII4319	114	2	8.76	0.03
OII4366	102	4	8.62	0.07
OII4414	144	2	8.61	0.03
OII4416	124	8	8.70	0.12
OII4452	53	3	8.59	0.07
OII4638	109	2	8.94	0.04
OII4641	145	2	8.84	0.03
OII4650	159	4	8.62	0.06
OII4661	113	2	8.83	0.03
OII4673	44	5	8.81	0.13
OII4676	97	4	8.70	0.07
OII4696	30	3	8.74	0.10
OII6641	48	2	8.90	0.04
OII6721	69	2	8.79	0.03
OII4072	113	7	8.65	0.13
OII4076	133	4	8.70	0.07
OII4078	56	3	8.77	0.08
OII4086	68	6	8.83	0.14
OII4891	34	3	8.67	0.09
OII4906	53	3	8.67	0.07
OII4941	48	2	8.54	0.04
OII4943	68	3	8.57	0.06
OII4956	24	3	8.77	0.11
			ϵ_O **= 8.71**	$\Delta\epsilon_O(\sigma) = 0.10$
	$\Delta\xi_t$(O) = 0.3		⇒	$\Delta\epsilon_O(\xi_t) = 0.04$

Table 11 Results from the abundance analysis of HD 36959 (B1 V)

HD 36959	T_{eff} = 25800 K, log g = 4.2 dex			ξ_t(Si)=0.0
Line	EW (mÅ)	ΔEW (mÅ)	ϵ_{Si} (dex)	$\Delta\epsilon_{Si}$ (dex)
SiII4128	16	3	7.52	0.12
SiII4130	17	3	7.44	0.12
SiIII4552	142	1	7.48	0.02
SiIII4567	124	1	7.48	0.02
SiIII4574	90	1	7.54	0.02
SiIII5739	99	2	7.51	0.04
SiIV4089	45	1	7.45	0.04
SiIV4116	36	3	7.47	0.12
			ϵ_{Si} **= 7.49**	$\Delta\epsilon_{Si}(\sigma) = 0.03$
	$\Delta\xi_t$(Si) = 0.5		⇒	$\Delta\epsilon_{Si}(\xi_t) = 0.07$
HD 36959	T_{eff} = 25800 K, log g = 4.2 dex			ξ_t(O)=2.1
OII3945	55	2	8.78	0.05
OII3954	73	2	8.69	0.04
OII3982	50	2	8.63	0.05
OII4317	98	6	8.76	0.10
OII4319	86	3	8.69	0.06
OII4366	81	5	8.62	0.10
OII4414	116	2	8.64	0.03
OII4416	99	3	8.72	0.05
OII4452	45	2	8.62	0.05
OII4641	113	2	8.75	0.04
OII4650	133	5	8.65	0.08
OII4661	89	2	8.76	0.04
OII4673	35	2	8.72	0.07
OII4676	75	3	8.61	0.07
OII4696	25	2	8.69	0.08
OII6641	30	2	8.78	0.06
OII6721	48	2	8.75	0.04
OII4072	94	6	8.72	0.13
OII4076	108	6	8.73	0.12
OII4078	46	3	8.80	0.09
OII4086	48	3	8.70	0.09
OII4891	26	2	8.67	0.07
OII4906	40	2	8.67	0.06
OII4941	39	2	8.62	0.06
OII4943	55	2	8.66	0.05
			ϵ_O **= 8.70**	$\Delta\epsilon_O(\sigma) = 0.02$
	$\Delta\xi_t$(O) = 0.4		⇒	$\Delta\epsilon_O(\xi_t) = 0.06$

Table 12 Results from the abundance analysis of HD 37744 (B1.5 V)

HD 37744	T_{eff} = 23800 K, log g = 4.1 dex			ξ_t(Si)=0.5
Line	EW (mÅ)	ΔEW (mÅ)	ϵ_{Si} (dex)	$\Delta\epsilon_{Si}$ (dex)
SiII3856	20	4	7.49	0.22
SiII6371	18	6	7.57	0.22
SiIII4552	147	3	7.57	0.05
SiIII4567	120	4	7.49	0.07
SiIII4574	88	4	7.59	0.09
SiIII5739	86	4	7.45	0.08
SiIV4116	23	4	7.56	0.26
			ϵ_{Si} = **7.53**	$\Delta\epsilon_{Si}(\sigma)$ = 0.05
	$\Delta\xi_t$(Si) = 0.5		⇒	$\Delta\epsilon_{Si}(\xi_t)$ = 0.04
HD 37744	T_{eff} = 23800 K, log g = 4.1 dex			ξ_t(O)=3.6
OII3945	45	5	8.73	0.13
OII3954	66	7	8.72	0.15
OII4317	72	7	8.60	0.13
OII4319	73	8	8.67	0.16
OII4366	67	6	8.56	0.13
OII4414	100	14	8.62	0.23
OII4416	76	7	8.59	0.14
OII4452	32	6	8.51	0.20
OII4641	99	5	8.76	0.09
OII4650	123	8	8.71	0.13
OII4661	79	5	8.81	0.10
OII4673	25	5	8.67	0.20
OII4676	71	6	8.76	0.13
OII4696	20	5	8.73	0.23
OII6721	33	7	8.74	0.19
OII4069	136	13	8.83	0.18
OII4078	36	6	8.71	0.21
OII4906	32	4	8.69	0.13
OII4941	30	5	8.62	0.17
OII4943	45	5	8.69	0.13
OII4956	14	3	8.79	0.17
			ϵ_O = **8.70**	$\Delta\epsilon_O(\sigma)$ = 0.07
	$\Delta\xi_t$(O) = 1.4		⇒	$\Delta\epsilon_O(\xi_t)$ = 0.06

Table 13 Results from the abundance analysis of HD 35299 (B1.5 V)

HD 35299	T_{eff} = 23700 K, log g = 4.2 dex			ξ_t(Si)=0.5
Line	EW (mÅ)	ΔEW (mÅ)	ϵ_{Si} (dex)	$\Delta\epsilon_{Si}$ (dex)
SiII3856	27	5	7.65	0.24
SiII3862	15	2	7.44	0.13
SiII6371	23	4	7.64	0.13
SiIII4552	133	5	7.45	0.08
SiIII4567	110	2	7.40	0.04
SiIII4574	79	2	7.50	0.05
SiIII5739	81	2	7.47	0.04
SiIV4089	26	1	7.59	0.06
SiIV4116	18	2	7.48	0.15
			ϵ_{Si} = **7.50**	$\Delta\epsilon_{Si}(\sigma)$ = 0.08
	$\Delta\xi_t$(Si) = 0.5		⇒	$\Delta\epsilon_{Si}(\xi_t)$ = 0.02
HD 35299	T_{eff} = 23700 K, log g = 4.2 dex			ξ_t(O)=2.8
OII3945	44	2	8.81	0.06
OII3954	59	2	8.72	0.05
OII3982	38	2	8.62	0.06
OII4317	78	5	8.80	0.09
OII4319	66	3	8.69	0.07
OII4366	61	3	8.59	0.07
OII4414	95	5	8.70	0.09
OII4416	80	2	8.77	0.04
OII4452	32	2	8.61	0.07
OII4641	91	5	8.79	0.10
OII4650	112	5	8.73	0.09
OII4661	68	3	8.77	0.07
OII4673	25	2	8.76	0.08
OII4676	59	2	8.68	0.05
OII4696	17	2	8.70	0.10
OII6641	18	2	8.82	0.09
OII6721	29	3	8.77	0.09
OII4072	82	3	8.81	0.07
OII4076	94	4	8.79	0.08
OII4078	35	2	8.79	0.07
OII4086	36	2	8.67	0.07
OII4891	16	3	8.64	0.16
OII4906	28	2	8.70	0.07
OII4941	25	2	8.59	0.08
OII4943	40	2	8.71	0.06
OII4956	12	2	8.78	0.13
			ϵ_O = **8.72**	$\Delta\epsilon_O(\sigma)$ = 0.07
	$\Delta\xi_t$(O) = 0.6		⇒	$\Delta\epsilon_O(\xi_t)$ = 0.03

Table 14 Results from the abundance analysis of HD 36285 (B2 V)

HD 36285	T_{eff} = 20600 K, log g = 4.0 dex			ξ_t(Si)=1.7
Line	EW (mÅ)	ΔEW (mÅ)	ϵ_{Si} (dex)	$\Delta\epsilon_{Si}$ (dex)
SiII3856	41	2	7.38	0.07
SiII3862	37	5	7.52	0.19
SiII6347	61	4	7.60	0.09
SiII6371	45	3	7.53	0.08
SiIII4552	110	1	7.49	0.02
SiIII4567	88	2	7.44	0.04
SiIII4574	59	1	7.51	0.03
SiIII5739	53	2	7.46	0.05
			ϵ_{Si} **= 7.49**	$\Delta\epsilon_{Si}(\sigma) = 0.06$
	$\Delta\xi_t$(Si) = 0.5		⇒	$\Delta\epsilon_{Si}(\xi_t) = 0.05$

HD 36285	T_{eff} = 20600 K, log g = 4.0 dex			ξ_t(O)=5.5
OII3945	26	3	8.79	0.12
OII3954	41	3	8.79	0.09
OII4317	46	5	8.74	0.12
OII4319	42	3	8.69	0.08
OII4366	42	4	8.65	0.11
OII4414	63	3	8.70	0.06
OII4416	50	3	8.74	0.07
OII4452	26	3	8.88	0.12
OII4638	46	3	8.94	0.08
OII4650	78	4	8.70	0.07
OII4661	46	2	8.80	0.05
OII4673	12	3	8.68	0.21
OII4676	36	3	8.66	0.09
OII6721	15	4	8.99	0.23
OII4069	81	6	8.86	0.10
OII4072	55	4	8.80	0.11
OII4078	24	4	8.91	0.19
OII4086	24	10	8.78	0.48
OII4906	16	3	8.85	0.17
OII4941	16	5	8.84	0.29
OII4943	25	3	8.91	0.12
			ϵ_O **= 8.80**	$\Delta\epsilon_O(\sigma) = 0.10$
	$\Delta\xi_t$(O) = 1.5		⇒	$\Delta\epsilon_O(\xi_t) = 0.06$

Table 15 Results from the abundance analysis of HD 35039 (B2 V)

HD 35039	T_{eff} = 19800 K, log g = 3.7 dex			ξ_t(Si)=3.3
Line	EW (mÅ)	ΔEW (mÅ)	ϵ_{Si} (dex)	$\Delta\epsilon_{Si}$ (dex)
SiII3856	61	2	7.63	0.06
SiII3862	45	5	7.54	0.15
SiII6347	75	10	7.51	0.17
SiII6371	55	2	7.46	0.04
SiIII4552	125	10	7.49	0.15
SiIII4567	103	5	7.47	0.09
SiIII4574	67	5	7.52	0.11
SiIII5739	69	5	7.58	0.10
			ϵ_{Si} **= 7.52**	$\Delta\epsilon_{Si}(\sigma) = 0.06$
	$\Delta\xi_t$(Si) = 1.0		⇒	$\Delta\epsilon_{Si}(\xi_t) = 0.08$

HD 35039	T_{eff} = 19800 K, log g = 3.7 dex			ξ_t(O)=5.3
OII3945	31	2	8.91	0.07
OII3954	41	2	8.79	0.06
OII3982	25	2	8.69	0.08
OII4317	50	6	8.80	0.14
OII4319	45	4	8.74	0.11
OII4414	64	2	8.72	0.04
OII4416	54	4	8.82	0.10
OII4641	64	3	8.80	0.07
OII4650	82	2	8.74	0.04
OII4661	46	3	8.79	0.08
OII4673	15	4	8.79	0.25
OII4676	39	2	8.71	0.06
OII4069	80	3	8.88	0.05
OII4072	59	3	8.91	0.08
OII4078	21	4	8.84	0.21
OII4086	25	4	8.84	0.18
OII4941	12	3	8.68	0.21
OII4943	21	3	8.81	0.14
			ϵ_O **= 8.79**	$\Delta\epsilon_O(\sigma) = 0.07$
	$\Delta\xi_t$(O) = 1.5		⇒	$\Delta\epsilon_O(\xi_t) = 0.07$

Table 16 Results from the abundance analysis of HD 36629 (B2 V)

HD 36629	T_{eff} = 20000 K, log g = 4.1 dex			ξ_t(Si)=1.0
Line	EW (mÅ)	ΔEW (mÅ)	ϵ_{Si} (dex)	$\Delta\epsilon_{Si}$ (dex)
SiII3856	52	2	7.58	0.07
SiII3862	42	2	7.55	0.08
SiII6347	65	3	7.62	0.07
SiII6371	48	2	7.53	0.06
SiIII4552	90	1	7.52	0.02
SiIII4567	73	1	7.49	0.02
SiIII4574	46	1	7.51	0.03
SiIII5739	42	2	7.53	0.06
			ϵ_{Si} = **7.54**	$\Delta\epsilon_{Si}(\sigma)$ = 0.04
	$\Delta\xi_t$(Si) = 0.5		⇒	$\Delta\epsilon_{Si}(\xi_t)$ = 0.05
HD 36629	T_{eff} = 20000 K, log g = 4.1 dex			ξ_t(O)=6.0
OII3945	24	2	8.91	0.09
OII3954	28	2	8.68	0.07
OII4317	37	3	8.77	0.09
OII4319	30	2	8.63	0.07
OII4366	30	2	8.59	0.07
OII4414	50	2	8.69	0.05
OII4416	40	2	8.75	0.06
OII4452	16	1	8.74	0.06
OII4638	36	1	8.95	0.03
OII4641	41	1	8.63	0.03
OII4650	59	3	8.65	0.07
OII4661	32	2	8.72	0.07
OII4673	11	3	8.82	0.23
OII4676	27	2	8.65	0.07
OII4069	64	3	8.88	0.06
OII4072	45	2	8.83	0.06
OII4076	55	3	8.85	0.08
OII4078	15	2	8.79	0.13
OII4943	16	3	8.83	0.17
			ϵ_O = **8.76**	$\Delta\epsilon_O(\sigma)$ = 0.10
	$\Delta\xi_t$(O) = 1.7		⇒	$\Delta\epsilon_O(\xi_t)$ = 0.06

Table 17 Results from the abundance analysis of HD 36430 (B2 V)

HD 36430	T_{eff} = 18400 K, log g = 4.1 dex			ξ_t(Si)=3.5
Line	EW (mÅ)	ΔEW (mÅ)	ϵ_{Si} (dex)	$\Delta\epsilon_{Si}$ (dex)
SiII3862	61	5	7.43	0.13
SiII6347	100	10	7.57	0.16
SiII6371	74	6	7.49	0.12
SiIII4552	77	3	7.55	0.06
SiIII4567	53	2	7.40	0.05
SiIII4574	28	5	7.37	0.19
SiIII5739	25	2	7.47	0.08
			ϵ_{Si} = **7.47**	$\Delta\epsilon_{Si}(\sigma)$ = 0.08
	$\Delta\xi_t$(Si) = 1.0		⇒	$\Delta\epsilon_{Si}(\xi_t)$ = 0.07
HD 36430	T_{eff} = 18400 K, log g = 4.1 dex			ξ_t(O)=6.3
OII3954	19	5	8.77	0.26
OII4317	20	5	8.75	0.24
OII4319	20	5	8.76	0.25
OII4366	18	4	8.64	0.21
OII4414	33	3	8.78	0.10
OII4416	26	7	8.85	0.29
OII4641	27	5	8.74	0.20
OII4650	36	2	8.66	0.06
OII4661	18	3	8.72	0.16
OII4676	18	4	8.78	0.21
OII4069	37	3	8.86	0.09
OII4072	27	4	8.82	0.18
			ϵ_O = **8.76**	$\Delta\epsilon_O(\sigma)$ = 0.07
	$\Delta\xi_t$(O) = 2.2		⇒	$\Delta\epsilon_O(\xi_t)$ = 0.08

Table 18 Results from the abundance analysis of HD 35912 (B2 V)

HD 35912	T_{eff} = 18500 K, log g = 4.0 dex			ξ_t(Si)=3.2
Line	EW (mÅ)	ΔEW (mÅ)	ϵ_{Si} (dex)	$\Delta\epsilon_{Si}$ (dex)
SiII3856	65	2	7.35	0.05
SiII3862	62	4	7.53	0.11
SiII6347	99	2	7.60	0.03
SiII6371	71	3	7.49	0.06
SiIII4552	77	2	7.48	0.04
SiIII4567	60	2	7.45	0.05
SiIII4574	35	1	7.47	0.03
SiIII5739	30	2	7.51	0.07
			ϵ_{Si} = **7.48**	$\Delta\epsilon_{Si}(\sigma)$ = 0.07
	$\Delta\xi_t$(Si) = 0.5		⇒	$\Delta\epsilon_{Si}(\xi_t)$ = 0.04
HD 35912	T_{eff} = 18500 K, log g = 4.0 dex			ξ_t(O)=6.3
OII3945	15	5	8.88	0.32
OII3954	22	4	8.79	0.18
OII4317	25	5	8.82	0.20
OII4319	21	3	8.70	0.14
OII4366	22	5	8.70	0.23
OII4414	34	4	8.72	0.13
OII4416	29	3	8.85	0.11
OII4650	42	2	8.70	0.06
OII4661	25	3	8.86	0.13
OII4676	17	4	8.65	0.22
OII4069	44	3	8.91	0.08
OII4072	33	3	8.91	0.12
			ϵ_O = **8.79**	$\Delta\epsilon_O(\sigma)$ = 0.09
	$\Delta\xi_t$(O) = 2.2		⇒	$\Delta\epsilon_O(\xi_t)$ = 0.08

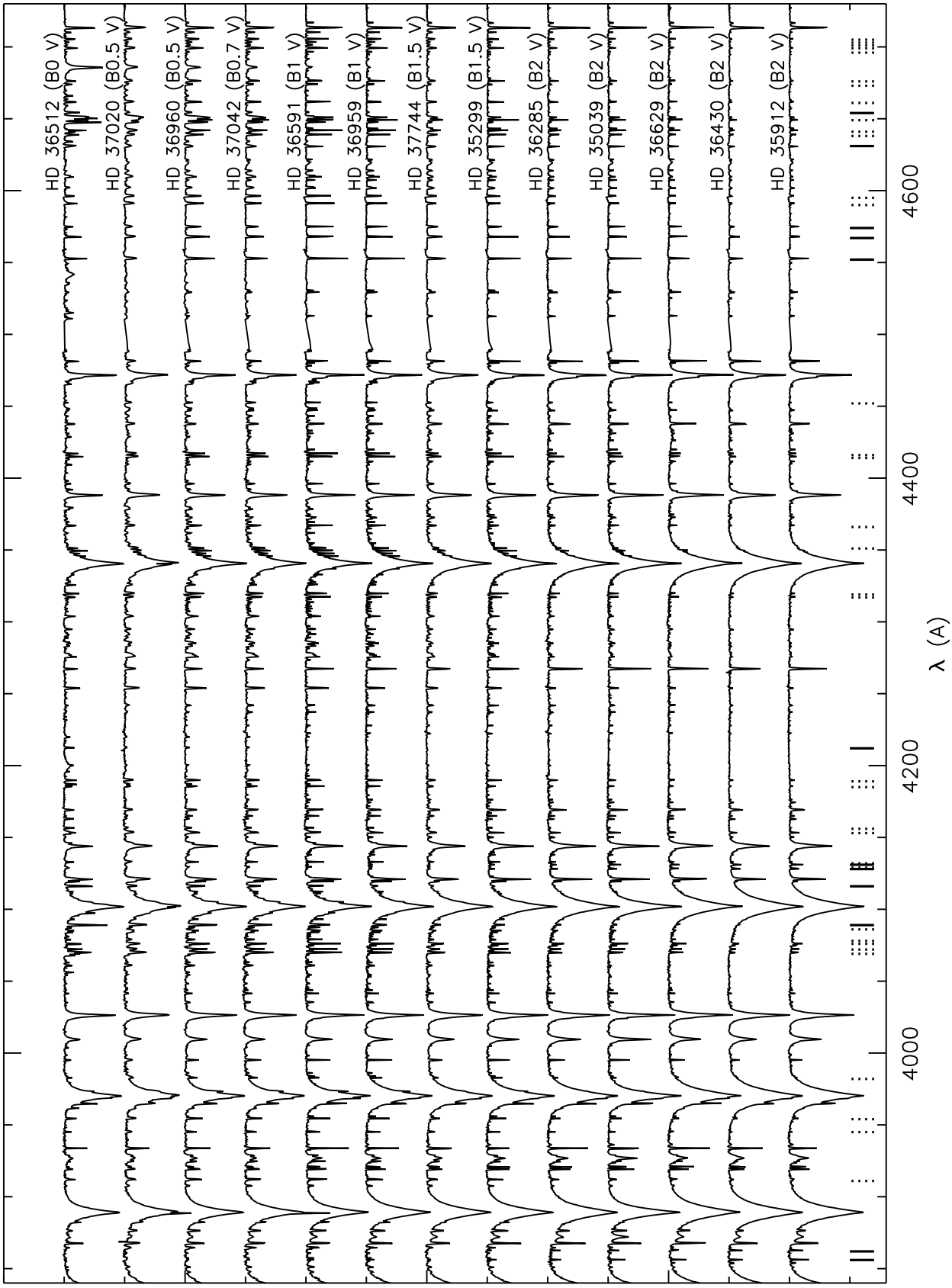

Fig. 8 The complete atlas of FIES@NOT spectra (part 1 of 3). The Si II-IV and O II lines used for the abundance analysis are indicated as solid and dashed vertical lines, respectively.

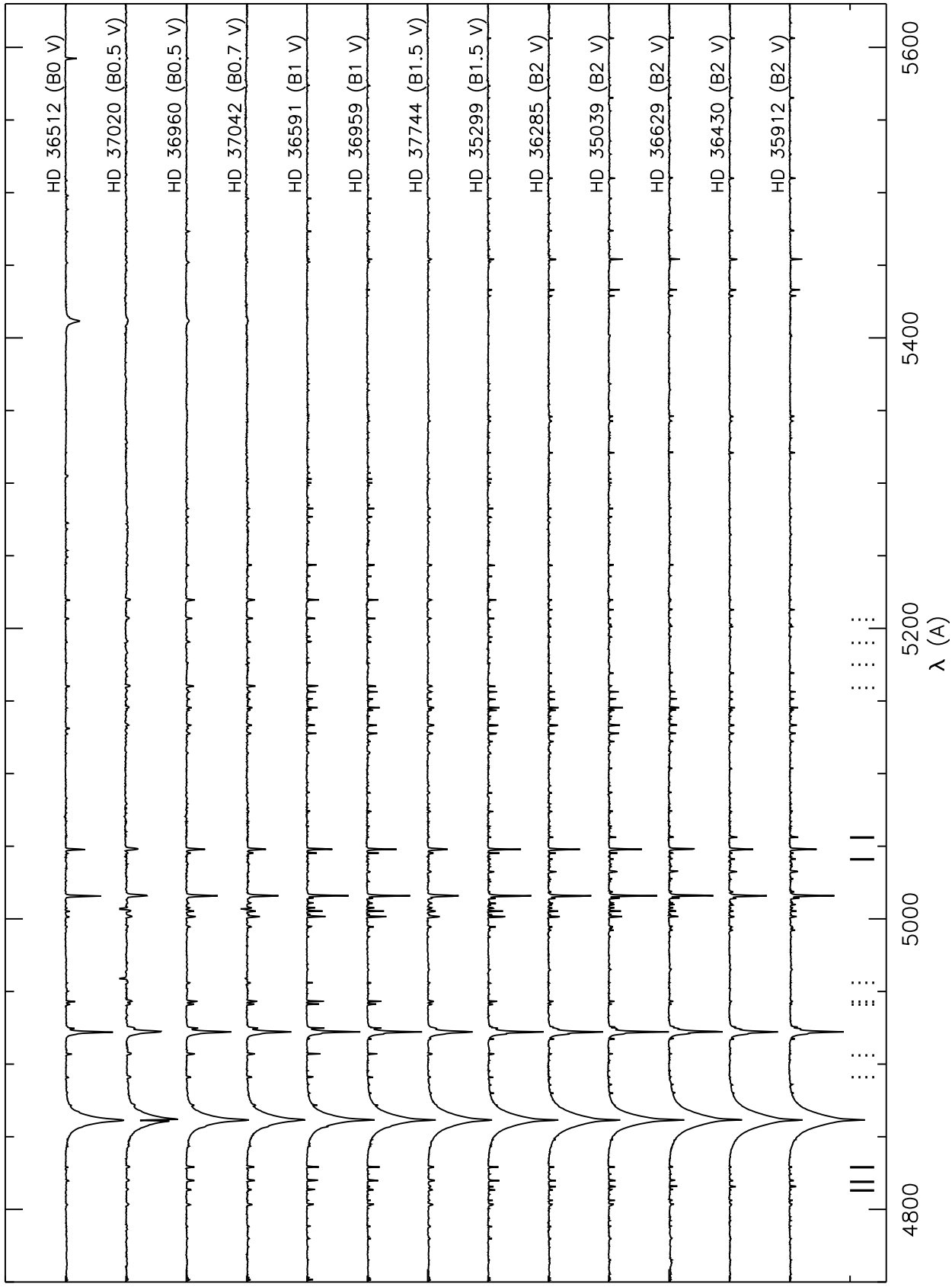

Fig. 9 The complete atlas of FIES@NOT spectra (part 2 of 3). The Si II-IV and O II lines used for the abundance analysis are indicated as solid and dashed vertical lines, respectively.

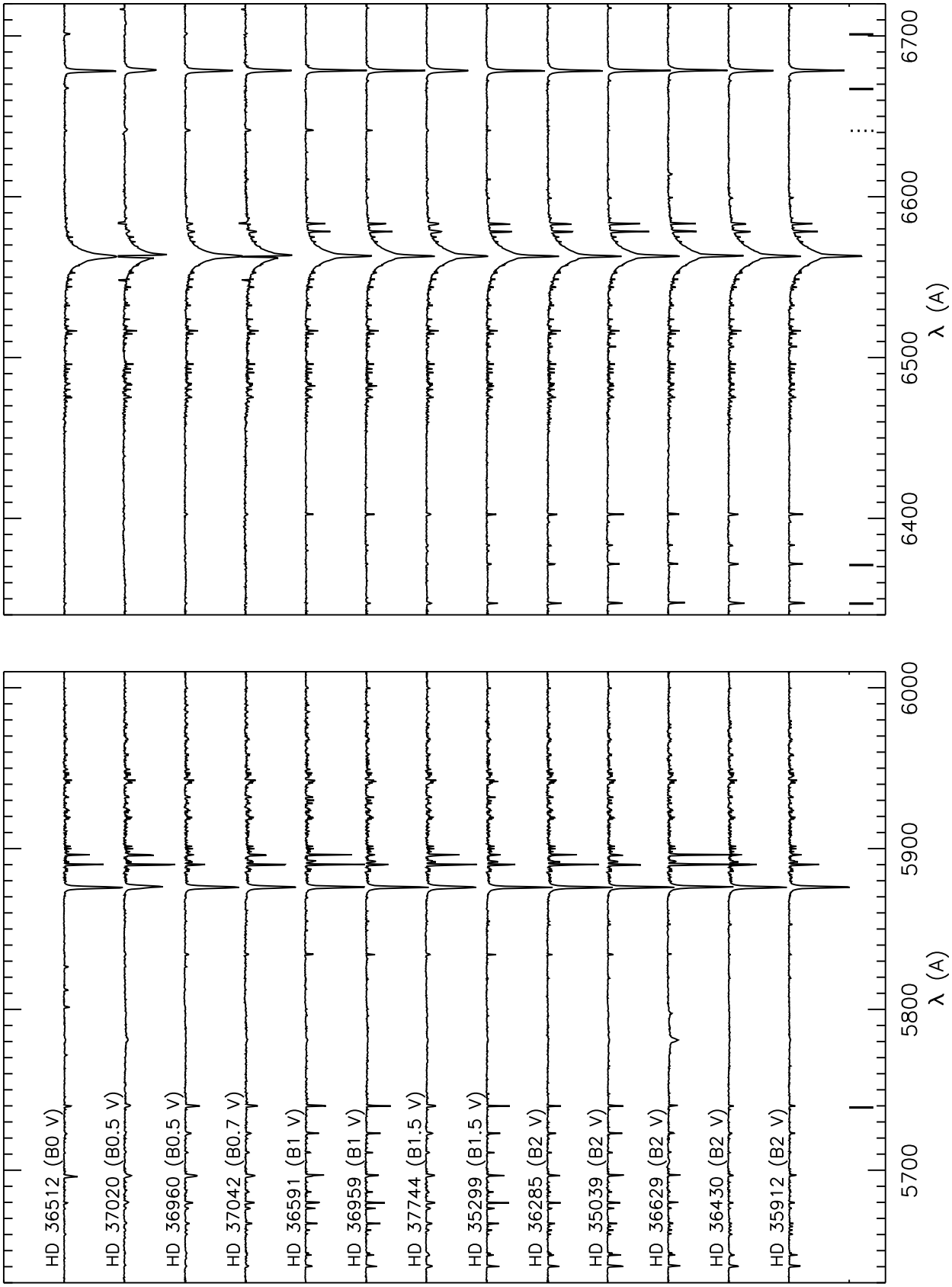

Fig. 10 The complete atlas of FIES@NOT spectra (part 3 of 3). The Si II-IV and O II lines used for the abundance analysis are indicated as solid and dashed vertical lines, respectively.